3D Printing of Metal-Organic-Framework (MOF) on Fishery Packaging for Real Time Freshness Monitoring

MS Thesis

by

Muhammad

CIIT/SP24-RPH-005/LHR

COMSATS University Islamabad, Lahore Campus

Pakistan

Fall 2025

3D Printing of Metal-Organic-Framework (MOF) on Fishery Packaging for Real Time Freshness Monitoring

A thesis submitted to

COMSATS University Islamabad, Lahore Campus

In partial fulfillment
of the requirements for the degree of

Master of Science

In

Physics

by

Muhammad

CIIT/SP24-RPH-005/LHR

Department of Physics

Faculty of Science

COMSATS University Islamabad, Lahore Campus

Pakistan

Fall 2025

3D Printing of Metal-Organic-Framework (MOF) on Fishery Packaging for Real Time Freshness Monitoring

This thesis is submitted to the Department of Physics in partial fulfillment of the requirements for the award of the degree of Master of Science in Physics

Name	Registration Number
Muhammad	CIIT/SP24-RPH-005/LHR

Supervisory Committee

Supervisor

Dr. Muhammad Ashfaq Ahmad
Professor
Department of Physics
COMSATS University Islamabad (CUI)
Lahore Campus

Co-Supervisor

Dr. Akhtar Hayat
Associate Professor
Department of IRCBM
COMSATS University Islamabad (CUI)
Lahore Campus

Certificate of Approval

This thesis titled

3D Printing of Metal-Organic-Framework (MOF) on Fishery Packaging for Real Time Freshness Monitoring

By

Muhammad
CIIT/SP24-RPH-005/LHR

has been approved

for the Degree of MS Physics

at COMSATS University Islamabad, Lahore Campus

External Examiner: _____

Supervisor: _____

Dr. Muhammad Ashfaq Ahmad
Department of Physics
CUI, Lahore

Head of Department: _____

Dr. Amir Razaq
Department of Physics
CUI, Lahore

Author's Declaration

I Muhammad, CIIT/SP24-RPH-005/LHR, hereby declare that I have produced the work presented in this thesis, during the scheduled period of study. I also declare that I have not taken any material from any source except referred to whatever due that amount of plagiarism is within an acceptable range. If a violation of HEC on this research has occurred in this thesis, I shall be liable to punishable action under the plagiarism rules of HEC.

Date: _____

_____

Muhammad
CIIT/SP24-RPH-005/LHR

Certificate

It is certified that Muhammad, CIIT/SP24-RPH-005/LHR, has carried out all the work related to this thesis under my supervision at the Department of Physics, COMSATS University Islamabad, Lahore campus and the work fulfills the requirements for the award of degree of MS in Physics.

Date: _____

Supervisor:

_____

Dr. Muhammad Ashfaq Ahmad

Professor

Department of Physics

COMSATS University Islamabad

Lahore Campus

Dedication

Dedicated to my parents, siblings, family, teachers, and friends for their support.

Acknowledgements

In the name of Allah, the most merciful and the kindest. Blessings be on Muhammad (PBUH), the messenger of Allah and the role model for mankind. I am thankful to Allah Almighty, who has created me, guided me, and given me intellectual properties. Without his blessings, I am nothing.

I am sincerely thankful to my supervisor, **Dr. Muhammad Ashfaq Ahmad**, for his guidance and kindness. His kind words gave me motivation. It was a privilege and honor to work under co-supervisor, **Dr. Akhtar Hayat**, whose constructive criticism and far-sightedness made me achieve this feet.

I would like to thank my group fellows **Ms. Saliha Gohar**, **Ms. Ayesha Tahira**, and **Ms. Husna Chaman** for their kind support and guidance. I am deeply thankful to my parents, siblings, and family for all their support, love and prayers.

Muhammad

CIIT/SP24-RPH-005/LHR

Abstract

3D Printing of Metal-Organic-Framework (MOF) on Fishery Packaging for Real Time Freshness Monitoring

By
Muhammad

The fabrication of colorimetric sensors via three-dimensional (3D) printing technology is an emerging field of research in recent times due to its cost-effectiveness, design freedom, and efficient use of sensing material. Herein, we utilize this technology to fabricate 3D printed multiplex tags (3D-PMTs) on textile fabric substrate to monitor real-time freshness of packaged fish. We prepare three sodium alginate (SA) based inks containing: rose anthocyanin incorporated metal-organic framework (RA-MOF) (pH indicator), curcumin incorporated metal-organic framework (Cur-MOF) (pH indicator), and silver nanoparticles (Ag NPs) (H_2S indicator), respectively. We demonstrate that the incorporation of these indicators into the cross-linked sodium alginate (SA) does not affect their colorimetric response towards pH change and H_2S. The 3D-PMTs exhibited excellent sensitivity, colorimetric response, and stability. These characteristics of the 3D-PMTs enable us to visually monitor the freshness of the packaged fish at three different storage temperatures (30°C, 16°C, and -4°C) for a prolonged period of time. The results demonstrate that these 3D-PMTs have great potential to be utilized in freshness monitoring.

Table of Contents

List of Figures

List of Tables

List of Abbreviations

3D	Three-Dimensional
3D-PMT	Three-Dimensionally Printed Multiplex Tag
MOF	Metal-Organic Framework
CD	Cyclodextrin
α-CD	Alpha-Cyclodextrin
β-CD	Beta-Cyclodextrin
ϒ-CD	Gama-Cyclodextrin
RA	Rose Anthocyanin
Cur	Curcumin
BTC	Trimesic Acid
DI	Deionized
DMF	Dimethylformamide
H_2S (aq.)	Aqueous Hydrogen Sulfide
SA	Sodium alginate
$CaCl_2$	Calcium Chloride
$NaHCO_3$	Sodium bicarbonate
NH_4OH	Ammonium Hydroxide
MeOH	Methanol
EtOH	Ethanol
Ag NPs	Silver nanoparticles
Na- β-CD-BTC-MOF	Sodium/ Beta-cyclodextrin/ Trimesic acid based MOF
FTIR	Fourier Transformed Infrared
XRD	X-Ray Diffraction
Cu Kα	Copper K-alpha
FE-SEM	Field Emission Scanning Electron Microscope
UV–Vis	Ultraviolet–Visible
rpm	Revolution per minute
RGB	Red Green Blue

Chapter 1
Introduction

1.1 Three-Dimensional (3D) Printing

3D printing or additive manufacturing is an emerging technology based on digital models, which are printed layer by layer to create a final product [1]. 3D printing technology has a great impact on science and has transformed the engineering of material science [2]. 3D printing offers improved resource efficiency, large-scale manufacturing, design freedom, minimal human effort, and uniformity compared to traditional methods [3, 4]. The structures to be printed are modeled using computer-aided design (CAD) software. The 3D models need to be converted into the STL file format, which is then sliced by 3D printer software in a series of 2D cross-sectional layers [5]. There are several techniques for 3D printing:

- Fused Deposition Modeling (FDM)
- Direct Ink Writing (DIW)
- Inkjet Printing
- Selective Laser Sintering (SLS)
- Stereolithography (SLA)

1.1.1 Fused Deposition Modeling (FDM)

In this technique, filaments or wires of thermoplastic polymers are melted through a hot nozzle and then the printed structure is cooled naturally to solidify it. This method has a range of applications from robotics to microfluidics. The resolution of printed structures depends not only on nozzle size but also on viscosity and flow characteristics of the filaments. The choice of the filament put a limit on resolution, surface finish, and porosity.

1.1.2 Direct Ink Writing (DIW)

This method is quite similar to FDM, requiring a viscoelastic ink that extrude through a nozzle under external pressure source. The ink is deposited on a substrate and the structure solidifies through either solvent evaporation, sudden change in stress, phase change or a combination of all these effects. This technique is extensively used by

researchers in making hydrogels used for drug delivery, soft robotics, sensors, and cellular structure applications. However, difficulty in making voids and hanging structures put some limits on its applications.

1.1.3 Inkjet Printing

In this technique, photopolymerizable resins is printed on a built plate by selectively placing pico-liter droplets. The printed structure is solidified using UV light source. The printed structure has better surface quality compared to DIW and FDM techniques. However, the cost of printers and resins are major limitations of this technique.

1.1.4 Selective Laser Sintering (SLS)

In this technique, a high power laser source at specific wavelengths is employed to irradiate a target powder beds such as metals, polymers, cement or ceramic, followed by sintering either through either through chemical or mechanical effects. The solidification process is faster compared to FDM or DIW. However, the surface finishing is often rough in this technique.

1.1.5 Stereolithography (SLA)

This technique is also known as light-based 3D printing. Photo-curable resins are employed in this technique which solidify through photochemical reactions. The structure is printed layer by layer. The first layer is solidified on a build plate and the proceeding layers are stacked and solidified layer by layer on the proceeding layer [6].

1.2 Metal Organic Framework (MOF)

MOFs are an emerging class of porous crystalline materials having enormous surface areas, making them highly efficient in the field of clean energy storage, gas storage and separation [7]. Traditional porous material were either organic or non-organic and had some limitations in their use. Organic porous material such as activated carbon, although have high surface areas and great adsorption capacity but they lack orderliness. This put a limit to their use in gas storage and separation, purification of water, solvent removal and recovery. Whereas, inorganic materials such as zeolites are highly porous but during removal of template the framework often breaks. MOFs have advantage, having both the properties of organic and inorganic porous materials. They are not only stable but have ordered structures [8]. They are grown under specific synthesis conditions using bottom-up approach, in which metal and organic molecules

are forced to react [9]. Cyclodextrin (CD) are commonly being used as organic ligand as it is recognized as safe material to be used in food, cosmetic and pharmaceuticals. Due to the presence of repeated –OCCO– binding motifs on both the primary and secondary faces of these cyclic oligosaccharides, a series of MOFs have been synthesized with group 1A elements of periodic table [10]. At present, there are three types of CD being used as organic ligands α-CD, β-CD, and ϒ-CD. These oligosaccharides contain 6, 7, and 8 glucose units connected end to end by α-1, 4-glucoside bond, respectively. Although, they have similar structure but they differ in pore sizes. The pore sizes of α-CD, β-CD, and ϒ-CD are 5.7 Å, 7.8 Å, and 9.5 Å, respectively. CD-MOFs are now extensively being used in adsorption and removal of molecules, sensors, encapsulation, and food packaging, due to their excellent biocompatibility, controllable porosity, and high surface area [11]. Most common synthesis technique includes:

- Solvothermal
- Hydrothermal
- layer-by-layer growth
- Mechanochemical
- Electrochemical
- Ultrasonic

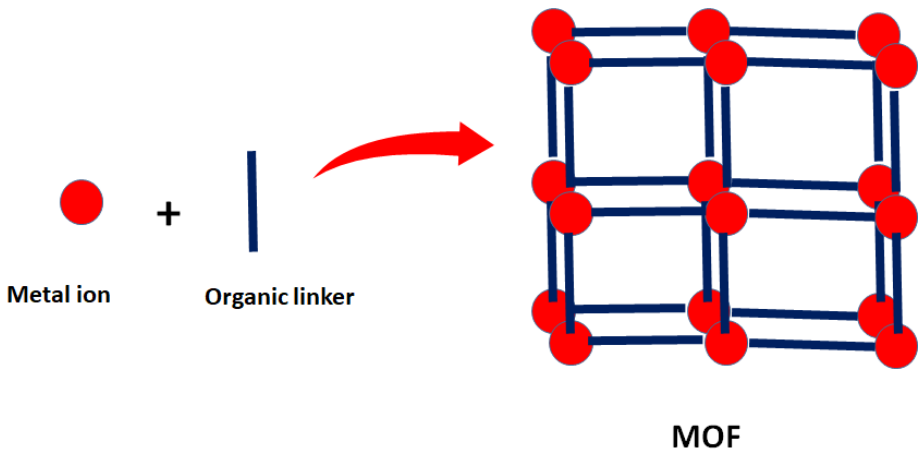

Figure 1.1 Schematic structure of Metal-Organic Framework (MOF)

1.3 Sensors

A sensor is device which detects or measures several chemical or physical properties of a compound such as temperature, pH, odor, pressure, light intensity, and so on by giving signals which are either human readable or can be machine readable [12].

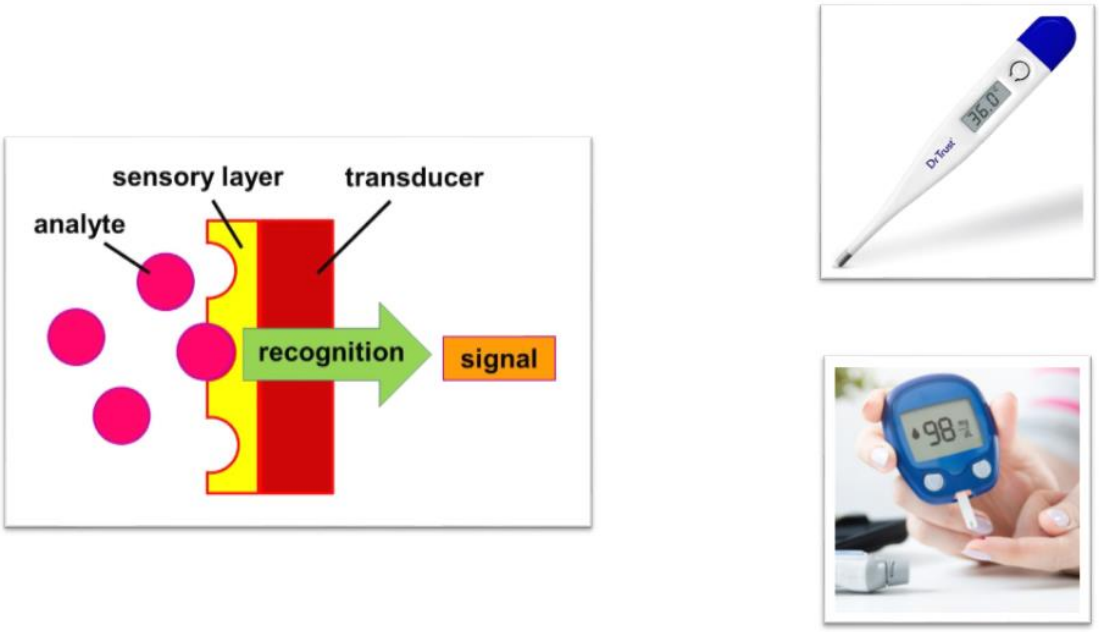

Figure 1.2: Illustration of the working of a sensor

Several types of sensors are being in daily life use [13]:

- Level Sensor
- Temperature Sensor
- Pressure Sensor
- Water Quality Sensor
- Chemical Sensor
- Gas Sensor
- Humidity Sensor
- pH Sensor

1.3.1 Level Sensor

It is type of sensor which is used to determine the amount of fluid or other substance flowing through a closed or open system. It has a variety of applications such as fuel gauging, sea level monitoring, and tsunami warnings.

1.3.2 Temperature Sensor

It is a commonly used sensor to monitor temperature variations and is utilized in air conditional control, agriculture sector, healthcare centers, and environment control devices.

1.3.3 Pressure Sensor

Is very essential device and is being utilized in pressure-driven systems where liquid pressure needs to be monitored continuously. If pressure limit exceeds, the sensor sends alarming signal to administrators.

1.3.4 Water Quality Sensor

Water is extremely essential liquid for the survival of living beings. Therefore, its quality needs to be monitored. This type of sensor is employed to check the quality of water for any purpose of use. It detects contaminated and polluted water before distribution.

1.3.5 Chemical Sensor

This type of sensor is used in industrial sector to detect any change in liquid or chemicals in air. It is not only used to monitor environmental changes in large cities but also detects the harmful chemicals released by industries and explosives and radioactive radiations.

1.3.6 Gas Sensor

It is quite similar to the chemical sensor except it only detects gases and monitor air quality. It is used in coal mines, oil and gas industries, and laboratories to detect toxic gases released in industrial sector or any leakage of gas.

1.3.7 Humidity Sensor

It is used to monitor the quantity of water vapors in an environment. It has vast variety of applications in pharmaceutical industries, museums, stadiums, greenhouses, and hospitals.

1.3.8 pH Sensor

It is used to monitor the acidity or alkaline nature of fluids or environment. It is commonly used in industrial sectors and in laboratories to monitor the pH of solvents.

1.4 Fish Spoilage

Fish is not only a delicious food but also a source of essential fatty acids (omega-3) that help to control cholesterol levels, enhance cognitive functioning, and reduce the chances of stroke and other heart diseases [14]. It is a highly perishable food product, and spoilage starts rapidly due to microbial growth during the storage period [15, 16]. The spoilage of fish is caused by microbial growth, such as Gram-negative bacteria (Vibrionaceae, Pseudomonas spp., and Shewanella spp.). These metabolic organisms consume amino acids from fish, which results in the release of total volatile basic nitrogen (TVB-N) and compounds of sulfides [17]. During spoilage, the decarboxylation of amino acids produces biogenic amines such as histamine and tyramine, which are highly toxic non-volatile compounds [18]. With the increase in population density, the demand for fresh food supply is also increasing; therefore, its quality needs to be monitored regularly.

1.5 Fish Freshness Monitoring

As spoiled fish is extremely unhealthy to consume, its monitoring is of great importance not only for consumers but also for retailers and industry [19]. The challenge for the food industry has been to develop low-cost, reliable, and rapid methods to monitor food quality in real-time. Traditional chemical and spectral methods, such as the Kjeldahl method, FTIR, and NMR, provide precise and authentic results but have the following limitations:

- Time-consuming
- Laborious
- Expensive
- Require skilled operators
- Require advance instruments [20, 21]

Other novel sensor array technologies, such as electronic nose, electronic tongue, and olfaction visualization, are non-destructive and non-hazardous, but have the following limitations in applying on a large scale: the efficiency of the electronic nose method decreases in a moist environment, the electronic tongue method requires liquid samples for online testing, and the olfaction visualization is time-consuming [22].

Colorimetric smart packaging-based sensors are used as an alternative to traditional methods due to their low cost, real-time, rapid, and non-destructive method to visually indicate the freshness of the packaged food [19]. They are being manufactured through casting, mixed extrusion, electrostatic spinning, and molding [23]. These sensors are composed of two main parts:

- A colorimetric indicator, such as pigments
- A matrix material to hold these indicators [24]

Conventional synthetic pH-responsive dyes like bromophenol green and bromophenol blue pose serious health issues due to their toxic substances. Among all the dyes, natural pigments such as anthocyanins and curcumin are extensively used due to their non-toxicity and excellent pH-responsive behaviors, but they lack stability [25-28]. Recent studies have shown that the stability of natural pigments can be improved by incorporating them into metal-organic frameworks (MOFs) [29, 30]. The sensing mechanism is simple; the spoilage of fish results in the release of total volatile basic nitrogen (TVB-N) and compounds of sulfides [17]. The strong correlation between the TVB-N concentration and the pH of the packed fish can be used to monitor the shelf life of the product [31]. However, these traditional manufacturing procedures have several challenges, such as complex design processes, integrating multiple sensing materials, poor production flexibility, and environmental stability [32].

During the last decade, three-dimensional (3D) printing technology has evolved as an additive manufacturing technique not only in the field of bone repair and tissue engineering but also in the chemical sensor field. Among all the printing methods, the extrusion-based printing has emerged as a widely used technology [33]. Various factors, such as nozzle size, flow speed, density, and viscosity of the ink, affect the structure formation of the 3D model [34]. Therefore, optimizing the precise concentration of printable ink and material incorporation is an important aspect of a stable and sensitive 3D printed sensor.

1.6 Significance of this Work

Several 3D printed sensors have been reported to monitor fish freshness in real-time [23, 24, 31]. But to the best of our knowledge, no one has reported a 3D printed sensor based on multi-dye incorporated MOF to monitor fish freshness. As the spoilage of fish produces highly toxic biogenic amines such as histamine and tyramine, its quality should not be monitored based on a single parameter [18].

This work attempts to develop a low-cost, environment-friendly, stable, and sensitive multiplex tag via three-dimensional (3D) printing technology for real-time freshness monitoring of packaged fish. All the materials used for the 3D printing of the sensor are green, eco-friendly, and can be utilized for large-scale production. To fabricate the multiplex tag, we optimize the concentration of sodium alginate (SA) and cross-link it with calcium chloride ($CaCl_2$) to make a printable ink. However, low viscosity and poor mechanical strength of alginate gels put a limit on their use in 3D printing [31, 35]. To overcome this challenge, we utilize a fabric substrate to enhance the mechanical strength and to minimize the spreading of the ink before stabilizing.

Herein, we utilize rose anthocyanin (RA) and curcumin (Cur) as pH-responsive dyes and incorporate these into MOF to prepare two different pH-responsive materials, RA-MOF and Cur-MOF, whereas silver nanoparticles (Ag NPs) are used as the hydrogen sulfide sensors. We prepare three inks using SA as a dispersion medium, containing two pH-sensitive materials (RA-MOF and Cur-MOF) and one hydrogen sulfide-sensitive material (Ag NPs). We hypothesize that by integrating multiple sensing materials, the freshness can be evaluated more efficiently, and by using a fabric substrate, the long-term stability of the 3D-PMTs can be improved.

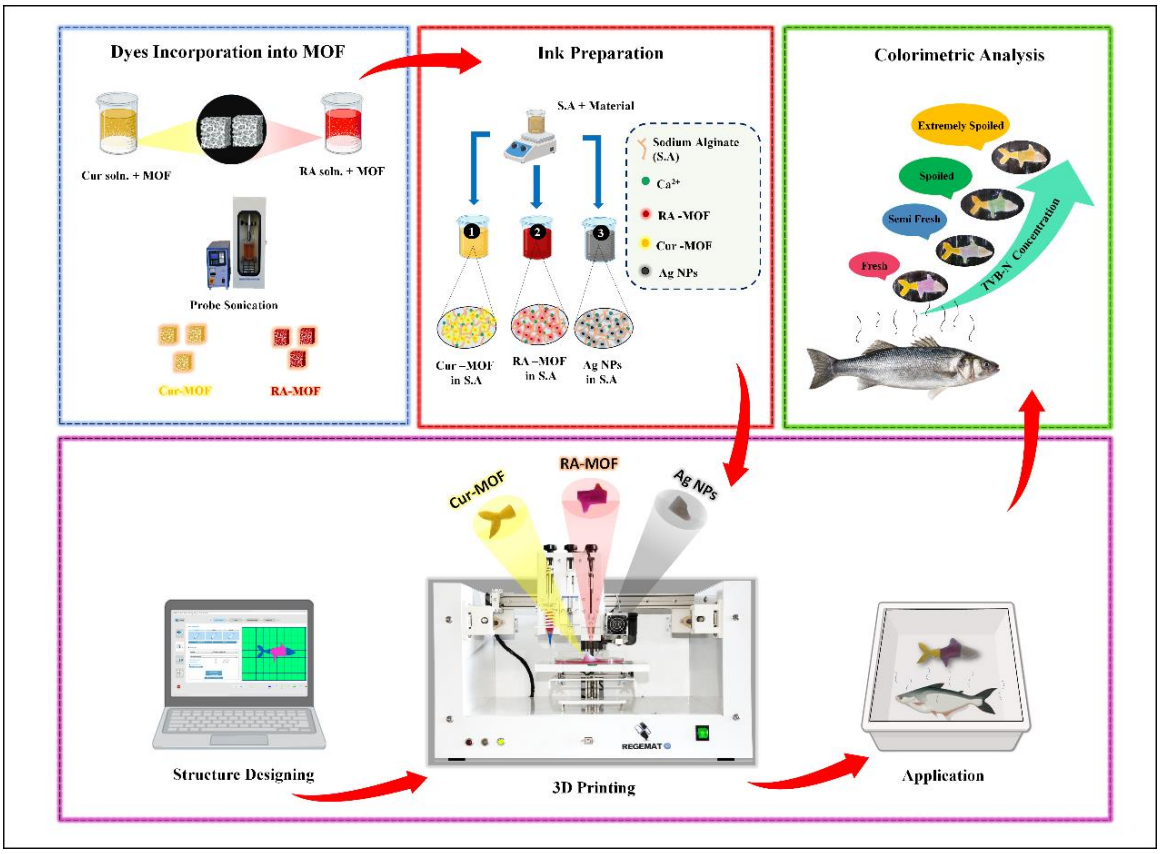

Figure 1.3: Schematic representation of the fabrication of a multiplex tag by 3D printing and its application in fish freshness monitoring

Chapter 2
Literature Review

Tang et al. synthesized a biopolymer-based pH responsive film using cobalt-based metal-organic framework (Co-MOF) attached with carboxymethyl cellulose (CMC) matrix. They tested the mechanical strength and colorimetric response of the film. When exposed to volatile ammonia, the Co-MOF nanoparticles first had a bright purple color before rapidly becoming brown. Further tests for real time freshness monitoring showed excellent discoloration of the film in reaction with ammonia [36].

Xu et al. developed a stable ammonia active film to monitor fish freshness by fabricating Copper-based framework nanocrystal employed with carboxymethyl starch/polyvinyl alcohol. Their blended film showed excellent mechanical strength, UV blockage and ammonia responsive color and stability [37].

Zhang et al. prepared aerogel colorimetric sensor for monitoring fish freshness by combining carboxymethyl cellulose (CMC) and anthocyanin in sodium alginate (SA) in different ratios. Their results showed that aerogel composite C/S/A1:2 demonstrated superior mechanical strength, the most uniform pore size, the highest specific surface area, and quick color changes in different alkaline vapors which could be employed as a non-destructive and useful smart sensor in monitoring the freshness of a variety of fish and meat [38].

Tang et al. developed a 3D printed pH-indicator film based on curcumin dye to monitor fish freshness. They prepared gel using curcumin, oregano oil Pickering emulsion, potato starch, and polyvinyl alcohol. They showed that the nozzle size effects the thickness of the film. They further emphasize the impact of 3D printing on food packaging [23].

Fang et al. prepared a pH indicator label using sodium alginate, UiO-66-NH_2 and red cabbage anthocyanin to monitor the initial spoilage of shrimp. The characterization results showed that the label performed well in minimizing anthocyanin leakage since

it demonstrated good UV absorption and durability. They tested the label in different pH environment and the label responded effectively by changing colors. Red cabbage anthocyanin color changed sequentially from red (acidic), to purple (neutral) and finally to yellowish green (basic) [39].

Chen et al. successfully prepared on package fish freshness indicator by making pH-responsive film containing curcumin and anthocyanin on a substrate based on starch, polyvinyl alcohol and glycerol. They tested the color stability and the result showed that when curcumin incorporated in the composite film it became more stable as compared to anthocyanin incorporated in then composite film (180 days). They further showed that when glycerol added to the film it became more sensitive to volatile ammonia. They suggested that this material could be used in intelligent packaging for on the spot non-destructive monitoring of fish products [28].

Tavakoli et al. fabricated smart films based on gelatin and soybean polysaccharides incorporated with mixed dyes (anthocyanin and phycocyanin) for non-destructive monitoring of spoilage of fish. They tested the film with single as well as mixed dyes and their result showed that the film prepared by incorporating the mixture of anthocyanin and phycocyanin exhibited the best color variation consistent with the degree of fish degradation [40].

Chapter 3
Materials and Methods

3.1 Chemicals and Reagents

Trimesic acid (BTC, 95%), beta-cyclodextrin (β-CD, 97%), calcium chloride anhydrous ($CaCl_2$, 90%), and hydrogen sulfide (aqueous) (H_2S, 99.5%) were obtained from Sigma-Aldrich. Sodium bicarbonate ($NaHCO_3$, 99%) was purchased from SAMCHUN. Dimethylformamide (DMF, 99.5%) and ammonium hydroxide (NH_4OH, 28%) were obtained from DAEJUNG. Sodium alginate was purchased from VWR BDH. Curcumin (Cur) was procured from Tokyo Chemical Industry (TCI). Methanol (MeOH, 99.99%) was obtained from Fisher Chemicals. Silver nanoparticles (Ag NPs) were previously prepared by our research group [41] . Absolute ethanol (EtOH) and fresh deionized water (DI water) were used in all experiments. Fresh red roses and textile fabric were obtained from the local markets of Lahore, Pakistan.

3.2 Instrumentation

Various advanced analytical instruments were utilized to obtain structural, morphological, and spectral characterization of the samples. The details are as follows:

- Structural Characterization of the samples was performed using Fourier Transformed Infrared (FTIR) spectroscopy in Attenuated Total Reflection mode (range = 4000–600 cm^{-1}) by a Nicolet 6700 FTIR spectrometer (Thermo Fischer Scientific, USA).
- Raman shift was measured at an excitation wavelength of 514 nm for 10 s using an InVia Raman Microscope (RENISHAW, UK).
- The X-Ray Diffraction peaks were obtained using a MiniFlex 600-C diffractometer (Rigaku, Japan) by means of Cu Kα radiations, over scan angle 2Θ = 5–50° with step size 0.02°.
- The surface morphological characterization was performed using Field Emission Scanning Electron Microscope (FE-SEM) Apreo S (Thermo Fischer Scientific, USA).
- The zeta potential of the samples was measured using Zetasizer Ver 7.12 (Malvern, UK).

- Ultraviolet–visible (UV–Vis) spectrum of the samples was obtained using a multi-plate reader MULTISCAN SKY (Thermo Fischer Scientific, USA).
- The color intensities were measured using a CAPSURE portable spectrocolorimeter (X-Rite PANTONE).
- A Smartphone was utilized to capture the colorimetric response of the sensor.

3.3 Synthesis of Na-β-CD-BTC-MOF

The MOF was synthesized using an ultrasonic-assisted method, as reported in the literature [42]. A probe sonicator (UH-250W) was employed in pulsed mode (2.0 s on/off). The procedure is as follows: 2g of β-CD and 70 mg of $NaHCO_3$ were added to a 50 mL beaker containing 10 mL of DI water. The mixture was then probe-sonicated for 10 min to obtain a homogeneous solution. 2g of Trimesic acid was then added to the solution for 24 h, followed by probe-sonication for another 10 min. The product was collected after centrifugation, washed with DMF, and subsequently dried in a drying oven at 50°C to yield MOF.

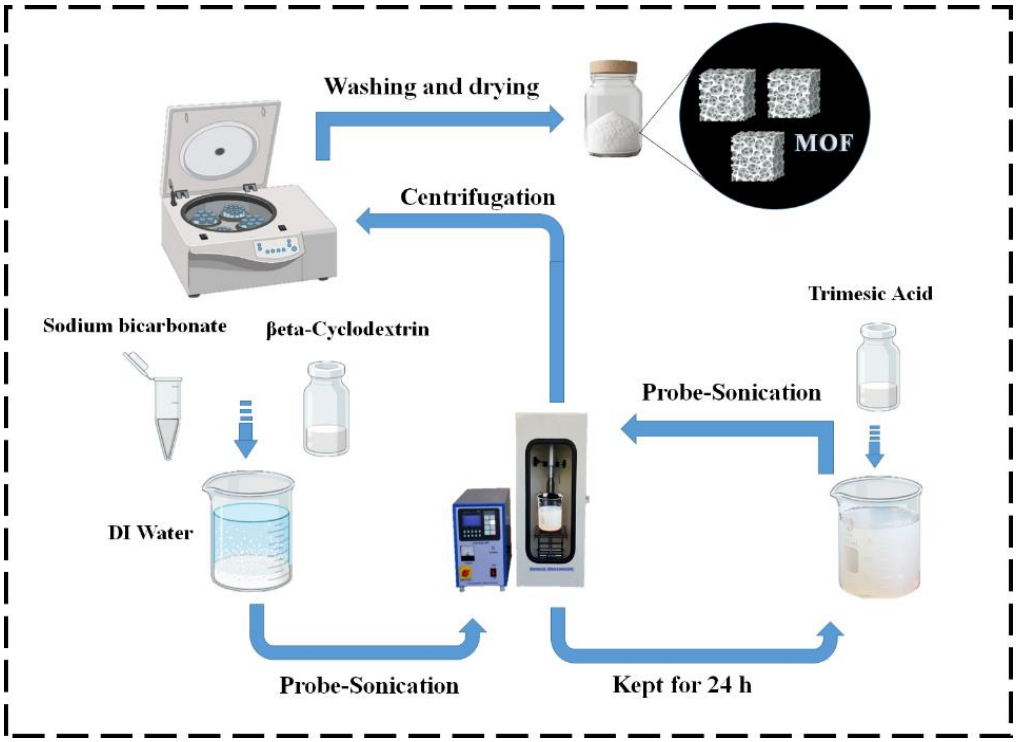

Figure 3.1: Schematic diagram of the synthesis of MOF

3.4 Extraction of Rose Anthocyanin

Rose anthocyanin (RA) was extracted by the solvent extraction method as reported previously in the literature [43]. Petals of fresh red roses were plucked and dried at 40°C in a drying oven. The dried rose petals were then ground into powder form, followed by the extraction process through magnetic stirring in a 500 mL beaker containing 200 mL of EtOH. The extraction process continued in the absence of daylight for 24 h at 40°C. The mixture was then filtered, and the filtrate was evaporated at 40°C, yielding RA.

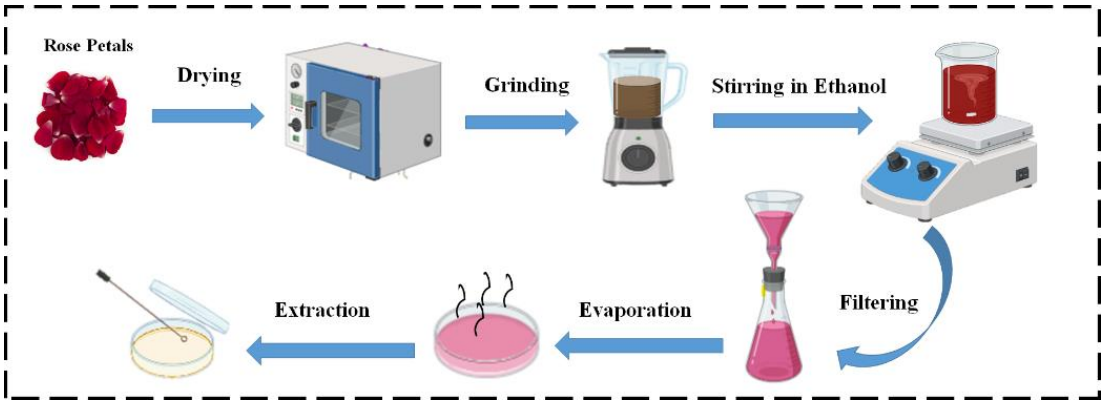

Figure 3.2: Schematic diagram of the extraction process of rose anthocyanin

3.5 Incorporation of Dyes into MOF

Two natural, pH-responsive dyes (anthocyanin and curcumin) were incorporated into the MOF to form two stable pH-responsive materials (RA-MOF and Cur-MOF). The procedure is as follows: 100 mg of previously prepared RA was added to a 10 mL beaker containing 2 mL of DI water to make the RA solution through continuous stirring (30°C, 80 rpm) for 1 hour. 50 mg of MOF was then added to the RA solution. The incorporation was facilitated by probe sonication for 20 minutes. The composite was then washed with methanol and dried at 50°C in a drying oven, yielding red colored RA-MOF.

The procedure for the Cur incorporation is slightly different; the Cur solution was prepared in absolute ethanol due to its low solubility in water. The procedure is as follows: 27 mg of Cur was dissolved in 10 mL of EtOH in a 25 mL beaker through continuous overnight stirring (30°C, 80 rpm) in a dark condition to make the Cur

solution. 200 mg of MOF was then added to the Cur solution and stirred (30°C, 80 rpm) for 3 hours. The incorporation was assisted by probe sonication for 7 minutes. The composite was then washed with methanol and dried at 50°C in a drying oven, yielding yellow colored Cur-MOF.

3.6 Preparation of 3D Printable Inks

Sodium alginate (SA) was used as a hydrogel due to its biocompatibility, hydrophilicity, and low cost. But its low viscosity puts a limit on its use in 3D printing. It is crosslinked with calcium chloride to improve its printability. The procedure is as follows: first, 5% (weight/volume) of SA gel was prepared by dissolving 1.5 g of SA into 30 mL of DI water through overnight stirring (30°C, 80 rpm) in a 50 mL beaker. The gel prepared was then crosslinked with 10 mL of $CaCl_2$ solution (60 mM) under constant stirring (30°C, 240 rpm). It was then stored in the freezer for two hours. Three different colorimetric inks were then prepared by mixing appropriate quantities of RA-MOF, Cur-MOF, and Ag NPS separately into the previously prepared crosslinked SA gel through magnetic stirring (30°C, 80 rpm) for 20 minutes. The air bubbles from the inks were removed by centrifugation at 2000 rpm for minutes.

Table 3.1: Materials quantity and corresponding sodium alginate volumes

Material	SA gel
RA-MOF (70 mg)	8 mL
Cur-MOF (50 mg)	7 mL
Ag NPs (0.5 mL)	6 mL

3.7 Preliminary Colorimetric Response of Inks on Fabric

The colorimetric response of the prepared inks was tested on a fabric substrate prior to 3D printing. Firstly, the circular pieces of fabric were dip-coated with the colorimetric inks and then air-dried in a fume hood for 15 minutes. Then the ink-coated fabric pieces were pipetted with buffer solutions of various pH (3.0–11.0) and H_2S (aq.). The colorimetric responses were captured and the corresponding RGB (Red, Blue, and Green color intensities) were recorded. The buffers detail is as follows:

Table 3.2: Buffer solutions and their pH

Buffer solution	pH
Citrate Buffer	3.0
Acetate Buffer	4.5
Citrate Buffer	6.0
Phosphate-Buffered Saline	7.0
Phosphate-Buffered Saline	7.5
Ammonium Buffer	10.0
Ammonium Buffer	11.0

3.8 Modeling and 3D Printing of Multiplex Tag

Firstly, a 3D model of the sensor was designed using Autodesk software (Tinkercad). It is a free software available online. Three structures were separately designed in a fish-like shape, representing the head, body, and tail of a fish. The models were then exported in an STL file format to the REGEMAT 3D V1 BIOPRINTER software (REGEMAT3D Designer) for slicing and printing the models. The structure parameters are as follows:

Table 3.3: Dimensions of the designed model

Structure	Dimensions
Head	0.3 mm × 14 mm × 10.4 mm
Body	0.3 mm × 20.9 mm × 26.6 mm
Tail	0.3 mm × 19.3 mm × 17 mm

The structures were printed separately on fabric substrates in two layers of thickness 0.15 mm. The printing process is as follows: First, the inks were loaded into 3-cc syringes and 0.41 mm nozzle was attached to it. Different flow speeds were tested and it was found that 1.5 mm/s was optimal for continuous and uniform deposition of the ink on the fabric substrate placed on a glass bed. After printing the structures, they were then crosslinked with $CaCl_2$ solution (200 mM) and dried at room temperature for stabilization.

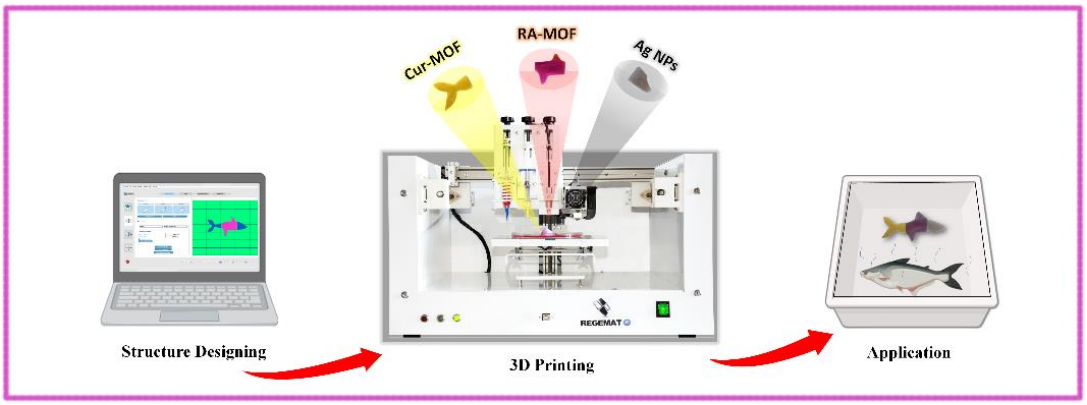

Figure 3.3: Modeling and 3D printing

3.9 Characteristics of 3D-PMTs

3.9.1 Colorimetric Response

The colorimetric response of the 3D-PMT was tested under simulated packaging conditions. The 3D-PMTs were affixed to the transparent cling films, covering the headspace of food packaging boxes (400 mL). Each box contained 3 mL of buffer solutions of different pH and H_2S (aq.) of varying volumes. The colorimetric response of the sensor was captured after three minutes of exposure.

3.9.2 Reactivity towards Ammonia and Hydrogen Sulfide

The reactivity test of the 3D-PMT toward ammonia and hydrogen sulfide was evaluated in a sealed environment. The 3D-PMT was first affixed to the inner side of a transparent cling film to cover a plastic food box (400 mL). Then, 1 mL of NH_4OH and 0.3 mL of aqueous H_2S (aq.) were added to the box. The head of the box was instantly covered with the cling film, exposing the 3D-MPT to the vapors. For a period of forty minutes at intervals of four minutes the color changes were captured along with their respective RGB values. The response sensitivity of the 3D-PMT was calculated according to the equation:

$$S\,(\%) = \frac{|R-Ro|+|G-Go|+|B-Bo|}{R+G+B} \times 100 \qquad (1)$$

The values R_o, G_o, and B_o are color intensities before the exposure, while R, G, and B are the color intensities after the exposure.

3.9.3 Stability Test of 3D-PMTs

The long-term stability of the 3D-PMT was evaluated over a period of four weeks. For this, four 3D-PMTs were stored in a dark condition at room temperature. One tag was tested each week to check precise colorimetric response by pipetting 1 mL of pH 11 buffer solution onto the tail (Cur-MOF), and the body (RA-MOF). While 1 mL of H_2S (aq.) was pipetted onto the head (Ag NPs). The colorimetric responses were captured within two minutes and Lab values were recorded to calculate total color difference ΔE values using the relation:

$$\Delta E = \sqrt{(L - L_o)^2 + (a - a_o)^2 + (b - b_o)^2} \quad (2)$$

Where, L_o (lightness), a_o (Redness-Greenness), and b_o (Yellowness-Blueness) represent the color parameters before exposure, while L, a, and b are the corresponding values after pipetting.

3.10 Real Sample Analysis

To check the practical applicability of 3D-PMTs to monitor real fish freshness, fresh fish pieces were placed in three plastic boxes. The boxes were then stored at three different temperatures (30° C, 16° C, and -4° C) after sealing with transparent cling films, to which 3D-PMTs were affixed on the inner side to avoid direct contact with the fish. The colorimetric responses of the 3D-PMTs were photographed at regular intervals to monitor changes corresponding to fish spoilage.

Chapter 4

Results and Discussions

4.1 Material Characterizations

4.1.1 X-Ray Diffraction (XRD)

The XRD pattern of MOF, RA, Cur, RA-MOF, and Cur-MOF was obtained to confirm the synthesis of MOF as well as incorporation of dyes into the MOF. The pristine MOF showed diffraction peaks at 2Θ = 6.34°, 10.76°, 12.6°, 18.06°, 19.24°, 22.64°, 24.18, and 27.00, which are consistent with the reported β-CD-based MOFs, confirming successful synthesis of MOF [44-47]. The diffraction peaks indicate the crystalline nature of MOF. Interestingly, the long-range crystallinity of the MOF was significantly suppressed in RA-MOF, indicated by the disappearance of sharp peaks. However, the presence of weak diffractions at 2Θ = 6.30°, 24.32°, and 26.58° indicated the MOF framework retention. The loss of long-range crystallinity and suppressed peaks can be attributed to both the incorporation of RA into the MOF cavities and their surface adsorption onto the framework. The diffraction peaks of Cur at 2Θ = 8.90°, 14.54°, and 25.58° disappeared in Cur-MOF, which can be attributed to the incorporation of Cur into the MOF cavities. The characteristic peaks of the pristine MOF at 6.3°, 10.64°, 12.64°, 18.78°, 19.48°, 24.18°, and 26.66° were retained with only a slight shift. The results indicate that the structural integrity of the MOF was preserved after incorporation of Cur.

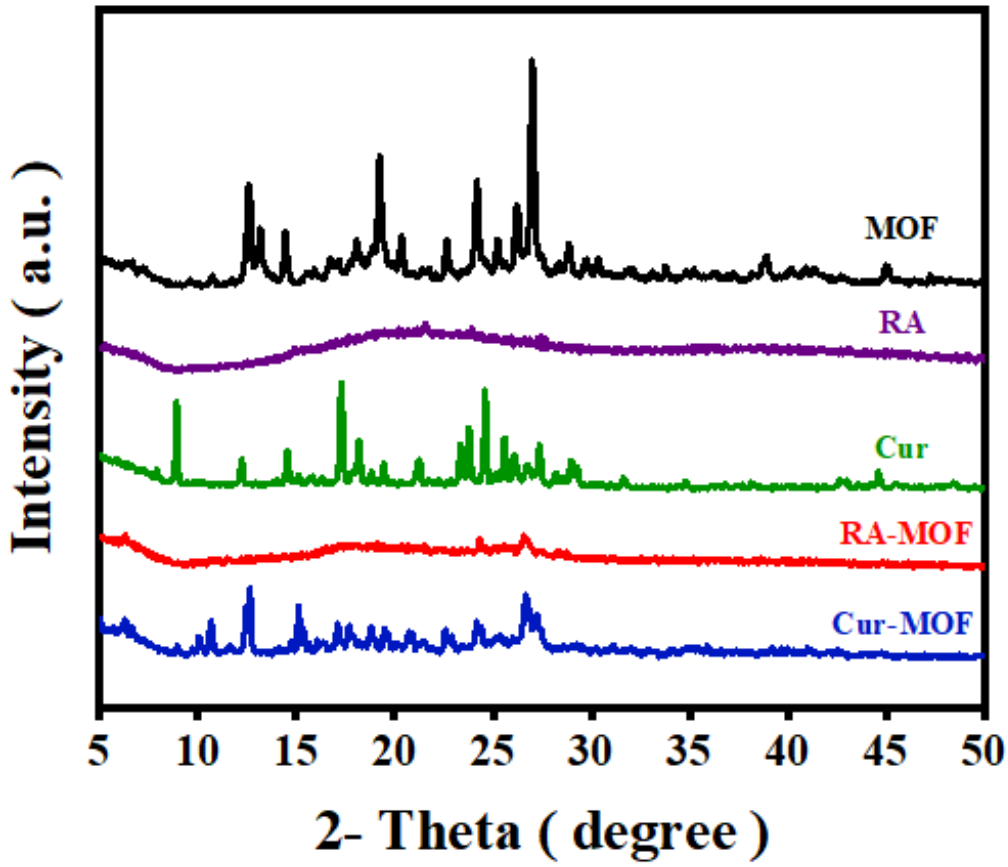

Figure 4.1: XRD pattern of MOF, RA, Cur, RA-MOF, and Cur-MOF

4.1.2 Raman Spectroscopy

Raman spectroscopy is versatile technique, based on inelastic light scattering, to analyze chemical structure, bonding and intermolecular interactions between the molecules. In this study, Raman spectroscopy was conducted to further analyze the host-guest interaction. The pristine MOF exhibited several characteristic vibrational modes. The low wavenumber vibrational modes at 202 and 376 cm^{-1} are assigned to Na–O vibrations, confirming the stable coordination between Na^{+} and organic linkers [48]. The band at 757 cm^{-1} corresponds to the in-plane deformation of glucose rings of β-CD. The C–O–C symmetric stretching mode, arising from the 1, 4-glycosidic bonds, appeared at 1004 cm^{-1} [49]. The mode at 1442 cm^{-1} is due to scissoring of $–CH_2$ bonds [50]. The bands appearing at 1623 and 1735 cm^{-1} are ascribed to C=O and O–C–O bonds of the BTC linker [51].

The slight shift in characteristic peaks and the appearance of new bands confirm the incorporation of RA into the MOF. The perturbation of characteristic vibrational bands of RA suggested the incorporation of RA into the MOF. The C–O stretching band of aromatic rings at 1274 cm^{-1} is shifted to 1301 cm^{-1}, indicating hydrogen bonding interactions between the host–guest molecules. Furthermore, the C=C stretching modes associated with phenyl rings and benzopyrylium moiety in the RA at 1499 cm^{-1} are shifted to 1496 cm^{-1}. This suggests the interactions with the organic linkers of MOF through π–π stacking [52]. The low wavenumber band appeared at 170 cm^{-1} is attributed to Na–O bond vibration, suggested the persistence of the MOF even after incorporation of RA.

Interestingly, the chemical structure of Cur was not affected by the incorporation, suggested by the retention of all characteristic vibrational bands of Cur. While the slight shifts in the peaks confirmed the strong host–guest interactions. The band associated with the enolic group C–OH stretching at 970 cm^{-1} is shifted to 974 cm^{-1}, while the C–H and C–O vibrations of the aromatic rings at 1256 cm^{-1} are shifted to 1287 $cm^{-1,}$ suggesting hydrogen bonding of Cur molecules with the MOF. The host–guest interaction was further confirmed by the shifting of inner ring chain vibrational band of C=O and C=C at 1618 cm^{-1} to 1623 cm^{-1}, suggesting the π–π stacking or electrostatic interactions [53, 54].

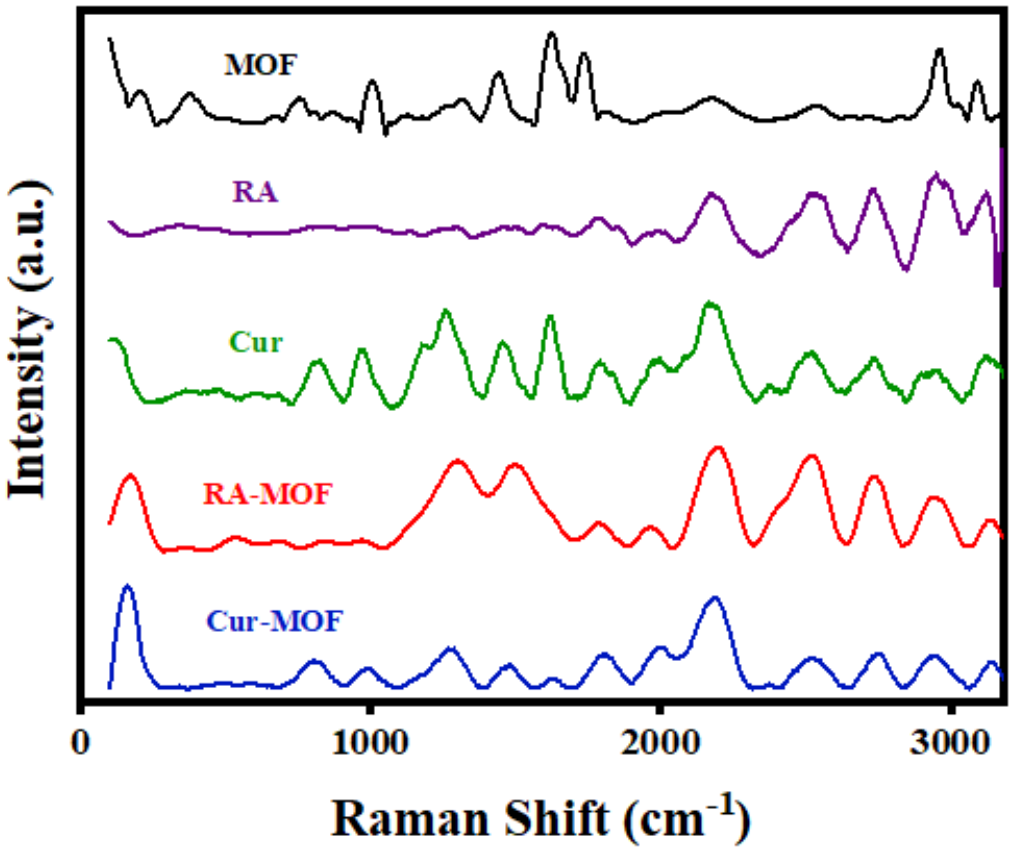

Figure 4.2: Raman spectra of MOF, RA, Cur, RA-MOF, and Cur-MOF

Table 4.1: Raman peaks analysis

Sample	Peak (cm^{-1})	Band association	Description
MOF	202, 376	Na–O	Coordination between metal ions and organic linkers
	757		In-plane deformation of glucose rings of β-CD
	1004	C–O–C	Symmetric stretching mode, arising from the 1, 4-glycosidic bonds
	1442	$–CH_2$	Scissoring vibrations
	1623	C=O	Bonds associated to BTC linker
	1735	O–C–O	
RA-MOF	170	Na–O	Retention of MOF even after incorporation
	1301	C–O	Stretching band of aromatic rings of RA
	1496	C=C	Stretching modes associated with phenyl rings and benzopyrylium moiety in the RA
RA-MOF	170	Na–O	Retention of MOF even after incorporation
	974	C–OH	Stretching of the enolic group of Cur
	1287	C–O, C–H	Vibrations of the aromatic rings
	1623	C=O, C=C	Inner ring chain vibrational band

4.1.3 Fourier Transformed Infrared Spectroscopy (FTIR)

The FTIR spectroscopy is another powerful characterization technique which is compliment of Raman spectroscopy to identify chemical bonds and functional groups in the sample. In this study, FTIR spectra of MOF, RA, Cur, RA-MOF, and Cur-MOF was obtained to study the incorporation effects. The symmetric O–H stretching in pristine MOF due to the presence of polysaccharides in β-CD was evidenced by broad peak around 3190 cm^{-1} [55]. The peak at 2927 cm^{-1} is attributed to C–H stretching vibrations. The number of peaks observed in the range 1718–1659 cm^{-1} are ascribed to the C=O vibrations from carboxyl groups present in BTC and O–H bending vibrations due to the existence of water molecules [46, 56]. The peak at 1388 cm^{-1} is assigned to O–H plane bending vibrations. The asymmetric and symmetric vibrations of C–O–C in the ring skeleton of the polysaccharides was confirmed by the peaks at 1150 cm^{-1} and 1024 cm^{-1}, respectively [42].

Interestingly, the incorporation of RA into the MOF resulted in a shift of the O–H stretching band from 3190 cm^{-1} to 3239 cm^{-1}, indicating the host–guest interaction such as hydrogen bonding between the hydroxyl groups of RA and the MOF. The host–guest interaction was further confirmed by the broadening of peaks representing C=O vibrations from carboxyl groups present in BTC from 1718–1659 cm^{-1} in pristine MOF to 1721–1604 cm^{-1} in RA-MOF.

The strong host-guest interactions after incorporation of Cur into the MOF was confirmed by spectral changes. Surprisingly, the free O–H stretching band at 3657 cm^{-1} in the Cur, disappeared when Cur was incorporated into the MOF. This suggested the hydrogen-bond formation between the Cur and MOF molecules [57]. Furthermore, the intensity of the symmetric O–H stretching band at 3190 cm^{-1} in pristine MOF decreases upon incorporation of Cur, due to host-guest interactions. The host-guest interactions was further confirmed by the shifting of the phenol group vibrational band C–O from 1274 cm^{-1} to 1265 cm^{-1}, when Cur was incorporated into the MOF [58].

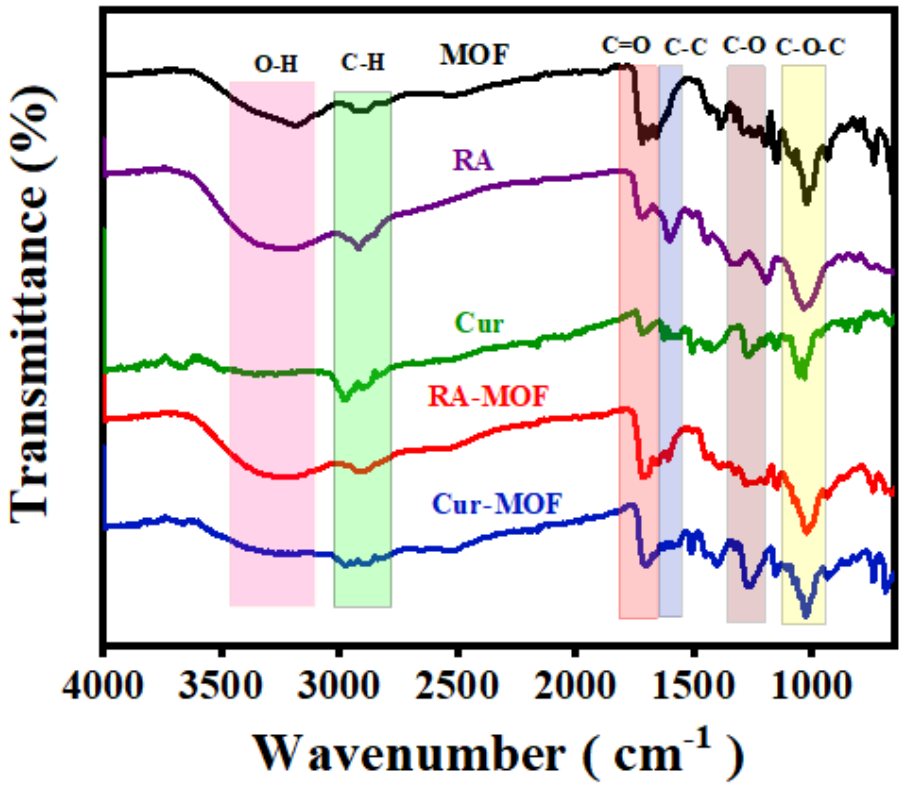

Figure 4.3: FTIR spectra of MOF, RA, Cur, RA-MOF, and Cur-MOF

4.1.4 Zeta Potential

The incorporation of dyes into the MOF was further confirmed by the zeta potential. The zeta potential of pristine MOF, RA, and Cur were 0.826 mV, 1.13 mV, and -14.7 mV, respectively. After incorporation of RA into the MOF, the zeta potential of MOF rises to 2.38 mV, confirming the successful incorporation of RA into the MOF. Surprisingly, the zeta potential of Cur remarkably dropped to -1.44 mV after incorporation into the MOF. The decrease in surface charge of Cur can be attributed to the host-guest interactions as indicated by Raman and FTIR analysis.

4.1.5 Field Emission Scanning Electron Microscope (FE-SEM)

FESEM was employed to visually confirm the incorporation of dyes into the MOF. The pristine MOF displayed a characteristic porous β-CD-based MOF structure. As indicated by XRD results, the RA incorporation resulted in a significant change in the surface morphology; the pores of the MOF appeared filled as well as the MOF surfaces coated with RA. This can be attributed to both the adsorption and the encapsulation of RA into the MOF cavities. As indicated by previous characterizations, the Cur-MOF displayed distinct morphological transformations due to strong host-guest interactions. The fine granules observed on the surface are attributed to the Cur coating over the MOF surface.

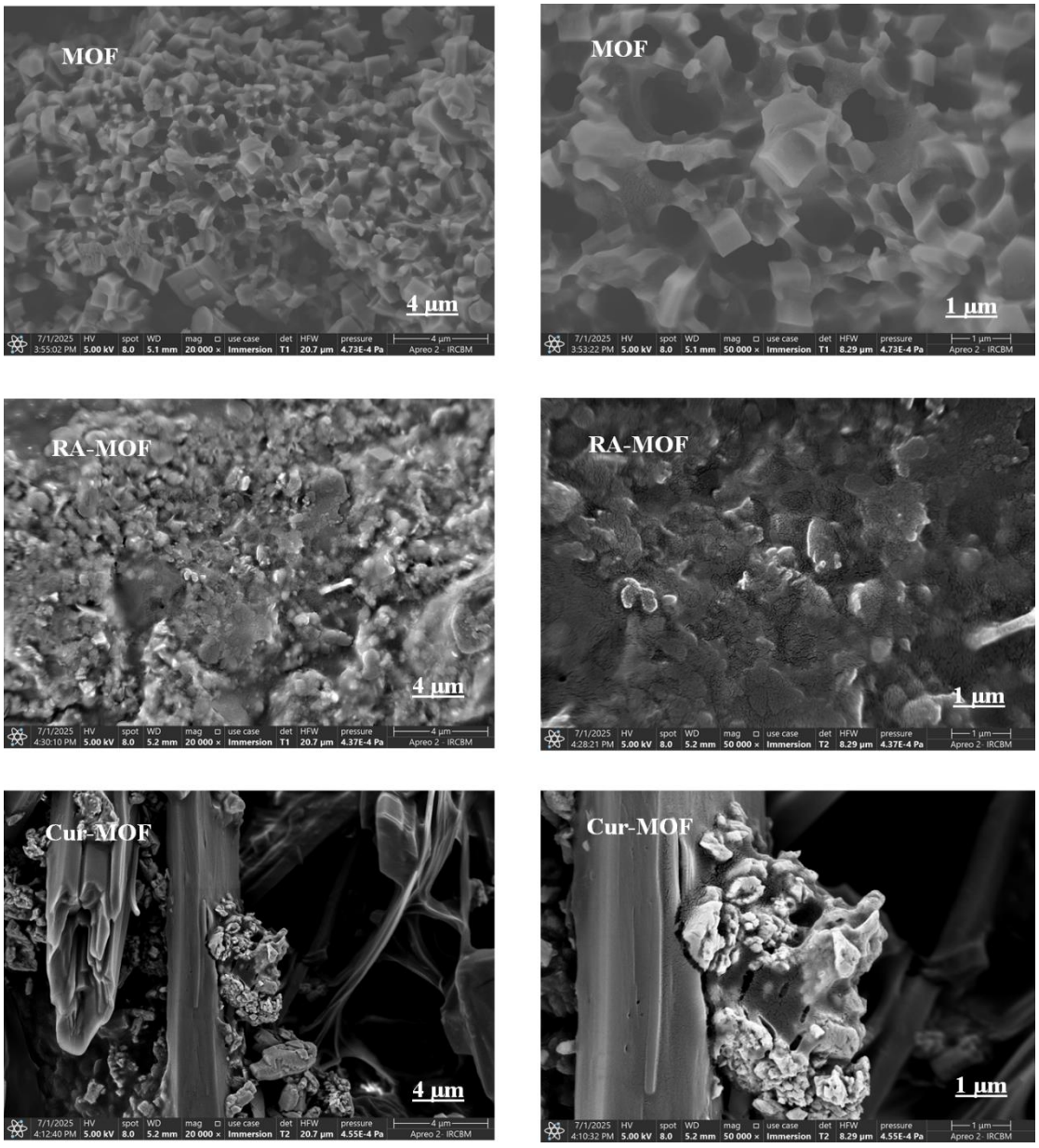

Figure 4.4: FESEM images of MOF, RA-MOF, and Cur-MOF

4.2 Ultraviolet–Visible Spectra (UV-Vis)

The UV-vis spectra of RA, RA-MOF, Cur, and Cur-MOF in buffer solutions of different pH (3.0–11.0) were obtained to compare color changing properties of dyes before and after incorporation. Surprisingly, the RA incorporated MOF displayed a remarkable enhancement not only in pH-responsivity but also the color transitions were increased compared to free RA. The RA-MOF suspension appeared pale pink at pH 3.0 (λ_{max} = 517 nm), colorless at pH 4.5 (no peak), dark pink at pH 6.0 (λ_{max} = 534 nm), violet at pH 7.0 (λ_{max} = 572 nm), purple at pH 7.5 (λ_{max} = 550 nm), sea green at pH 10.0 (λ_{max} = 591 nm), and green at pH 11.0 (λ_{max} = 596 nm). These distinct color transitions are due to the structural transformations of RA at different pH levels, from the flavylium cation to the carbinol pseudo base to the quinoidal base [59].

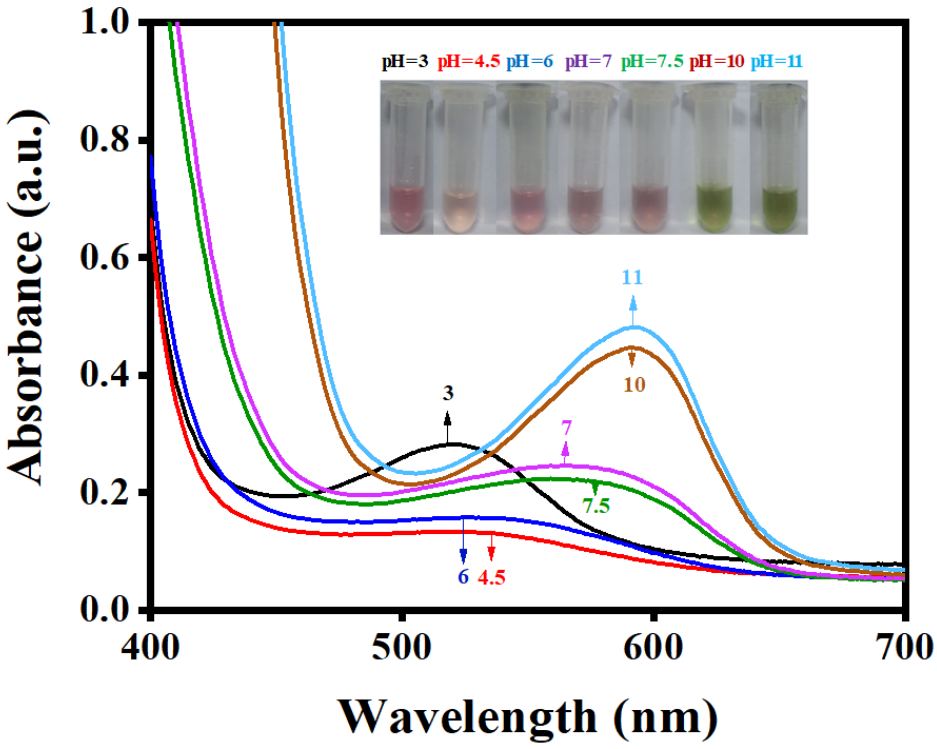

Figure 4.5: UV–vis spectra and color changes of RA in buffer solutions of different pH

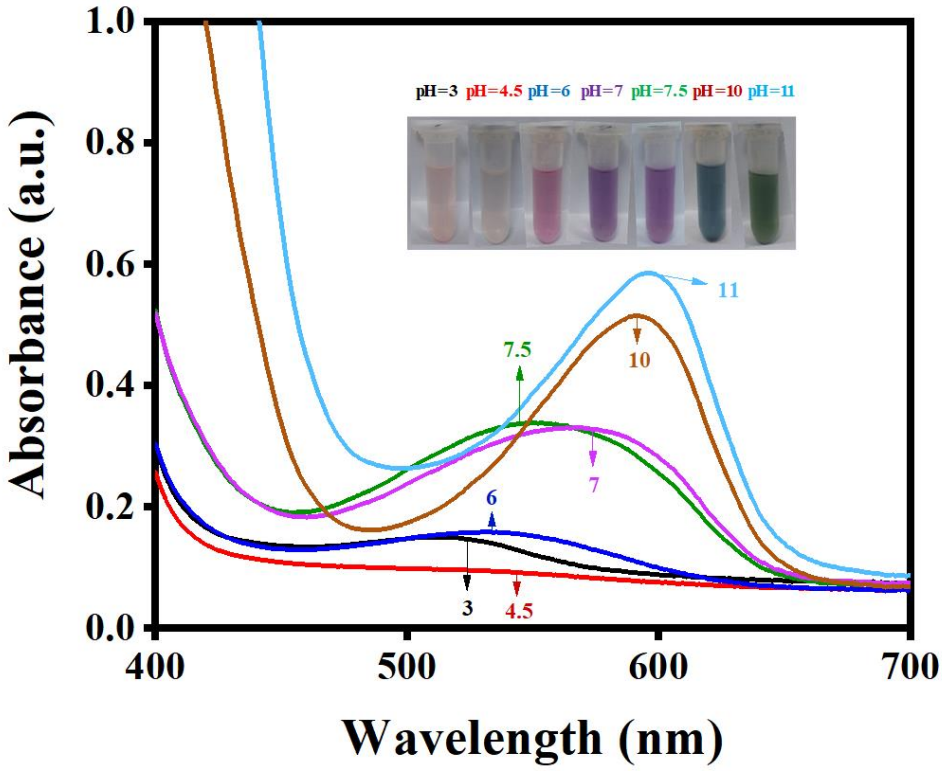

Figure 4.6: UV–vis spectra and color changes of RA-MOF in buffer solutions of different pH

Interestingly, the color intensity of Cur decreased when incorporation into the MOF compared to free Cur, at pH range 3.0–7.5. The Cur-MOF suspension appeared light yellow at pH 3.0–7.5 ($\lambda_{max} \approx 422$ nm). The decreased color intensity can be attributed to the limited π–π* electronic transitions of Cur within the pores of MOF [60]. The color intensity then drastically increases in alkaline conditions. The suspension appeared pumpkin orange at pH 10 ($\lambda_{max} = 427$ nm), and vivid orange at pH 11 ($\lambda_{max} = 434$ nm). The color transition is attributed to the structural transformation of Cur from keto form to the enol form [61].

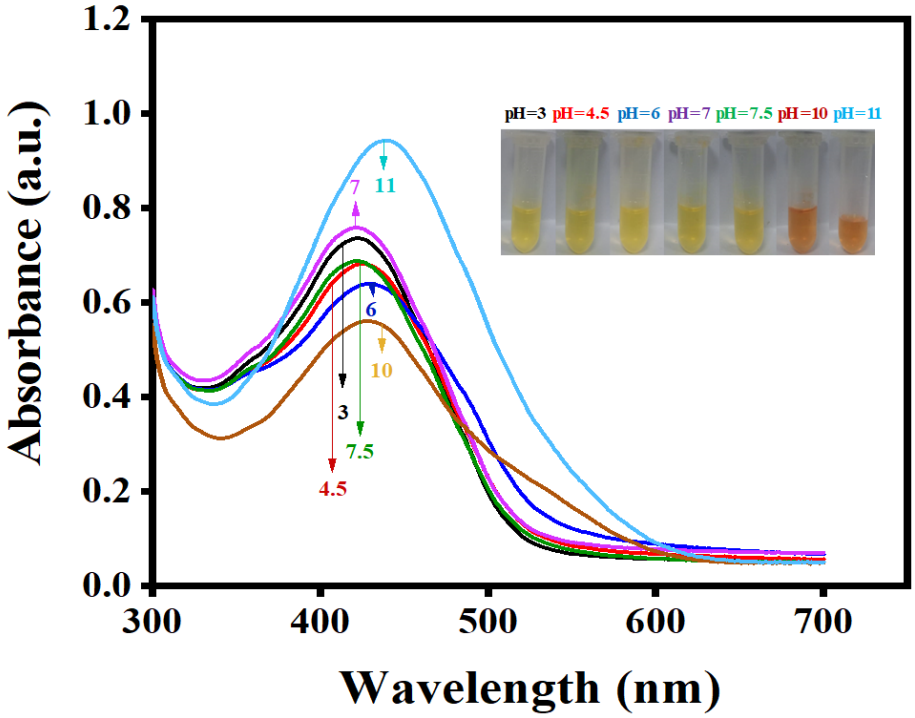

Figure 4.7: UV–vis spectra and color changes of Cur in buffer solutions of different pH

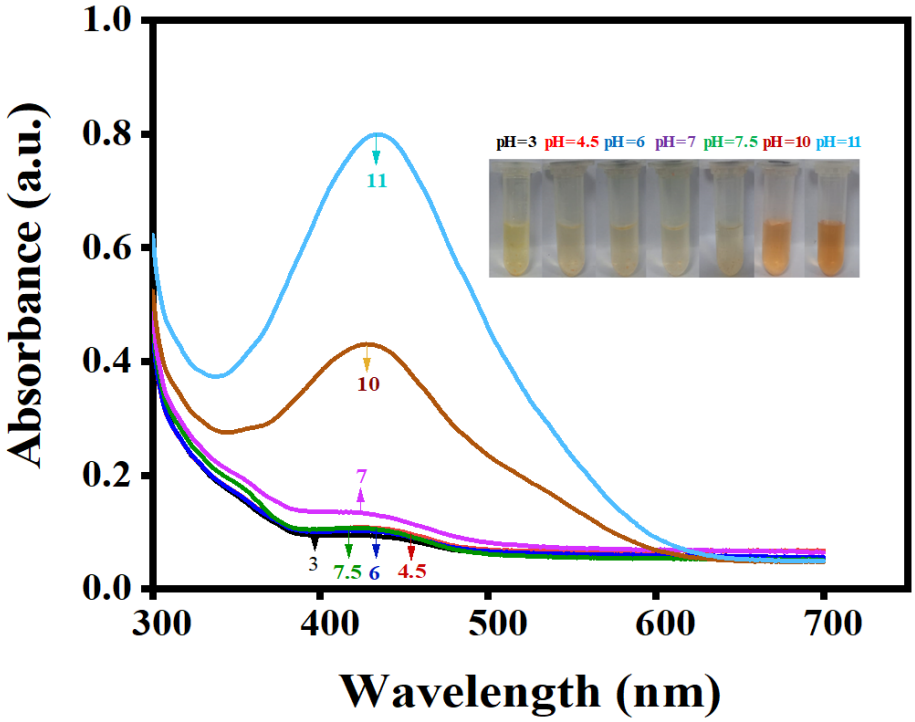

Figure 4.8: UV–vis spectra and color changes of Cur-MOF in buffer solutions of different pH

Ag NPs has a pronounced optical property Localized Surface Plasmon Resonance (LSPR) due to a collective oscillations of conducting electrons of Ag NPs when exposed to light. Due to this property an absorbance band appeared at 438 nm in UV-Vis spectrum of Ag NPs. In this study, Ag NPs were exposed to H_2S (aq.). This characteristic absorbance band of Ag NPs disappeared upon inclusion of H_2S (aq.), while the blackish-brown color of the Ag NPs dispersion changed to yellowish-brown. The results are ascribed to the interaction of Ag NPs with H_2S to form Ag_2S. The resulting Ag_2S shell on the Ag NPs' surface markedly suppresses the Localized Surface Plasmon Resonance (LSPR) of Ag NPs [62].

$$2Ag + H_2S \rightarrow Ag_2S + H_2 \quad (3)$$

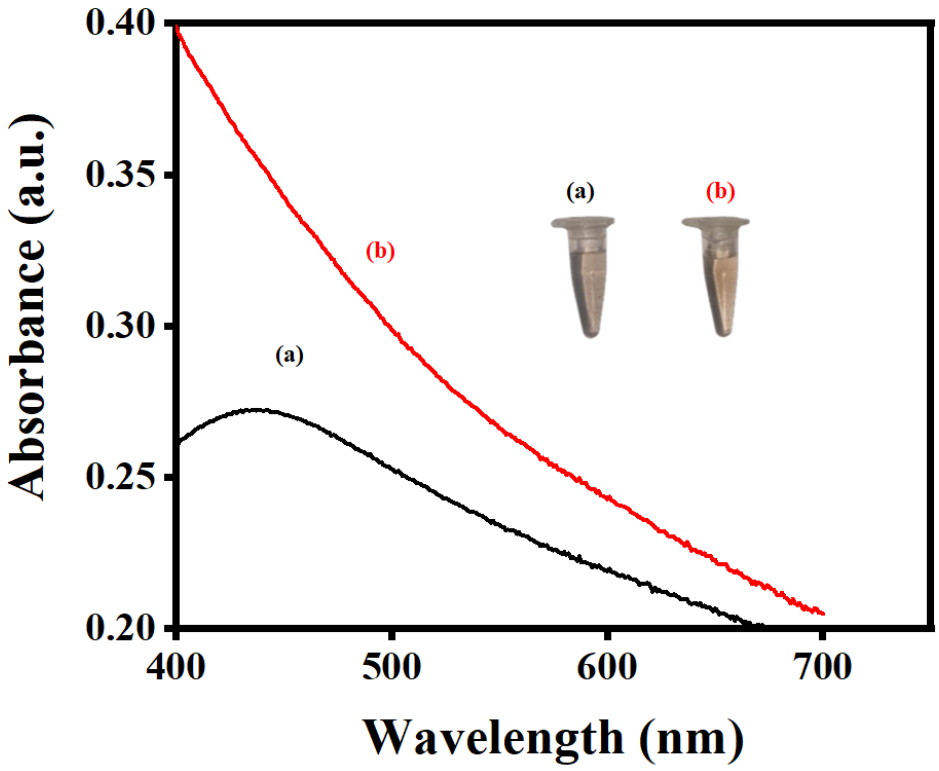

Figure 4.9: UV–vis spectra and color changes of Ag NPs (a) in the absence and (b) in the presence of H_2S

4.3 Preliminary Colorimetric Response of Inks on Fabric

After preparing the printable inks, we next analyzed their colorimetric response prior to 3D printing. The inks exhibited distinct color transitions upon exposure to different buffer solutions and H_2S (aq.). The results indicate that the incorporation of the RA-MOF, Cur-MOF, and Ag NPs in the SA gel matrix has not affected their corresponding sensing properties.

The figure below shows the colorimetric response and corresponding RGB values of the RA-MOF-coated fabric at different pH levels (3.0–11.0). With the increase in pH level (3.0–7.0), the R value decreases, corresponding to a visible color shift from red to pale pink. At pH 7.5, the B value increases, indicated by the appearance of a violet tone. At extreme alkaline conditions (pH = 10.0–11.0), the R value further decreases in comparison to the G and B values. The color appears sea green at pH 10.0 and Greenish at pH 11.0.

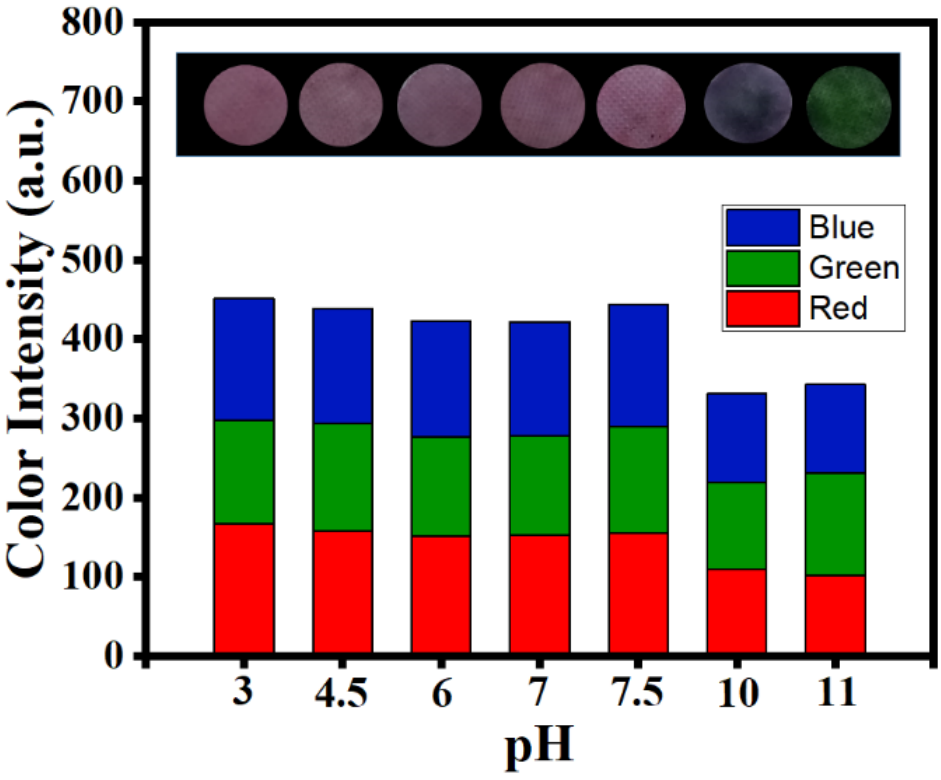

Figure 4.10: Evaluation of Red, Green, and Blue color properties of RA-MOF gel-coated fabric at different pH level

The Cur-MOF-coated fabric retained the pH-responsive properties, as shown in figure below. For pH values in the range 3.0–7.5, it appeared yellowish and then shifted to orange in alkaline conditions (pH = 10.0–11.0). Notably, the Cur-MOF-coated fabric exhibited the same trend as the Cur solution.

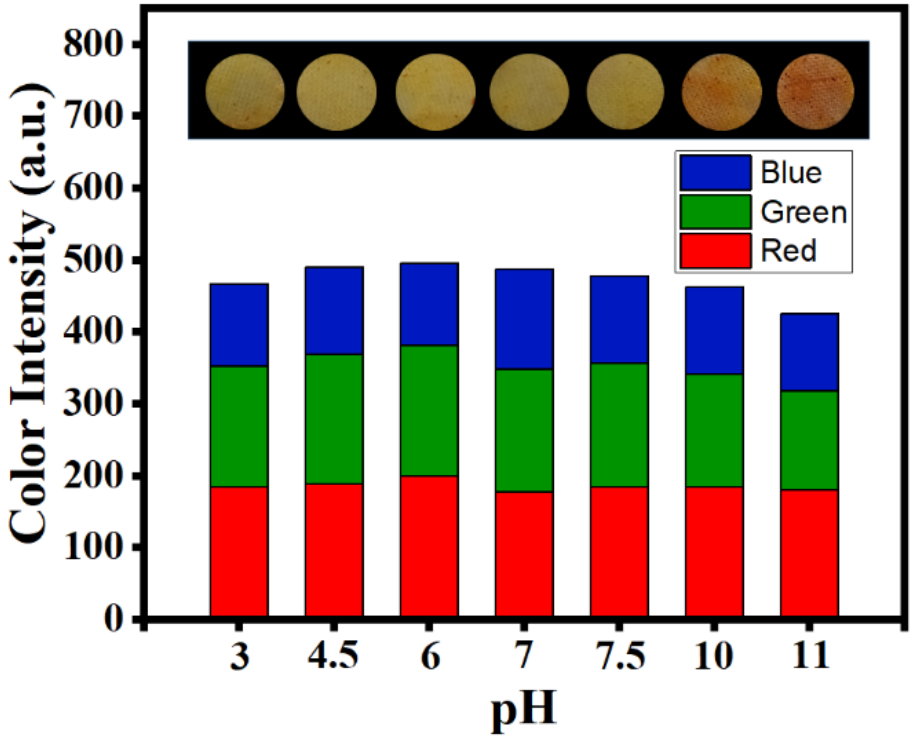

Figure 4.11: Evaluation of Red, Green, and Blue color properties of Cur-MOF gel-coated fabric at different pH level

The figure below shows the colors and RGB values of Ag NPs-coated fabric in the presence and absence of H_2S (aq.). The color of the Ag NPs-coated fabric transformed to brownish-yellow from whitish in the presence of H_2S (aq.).

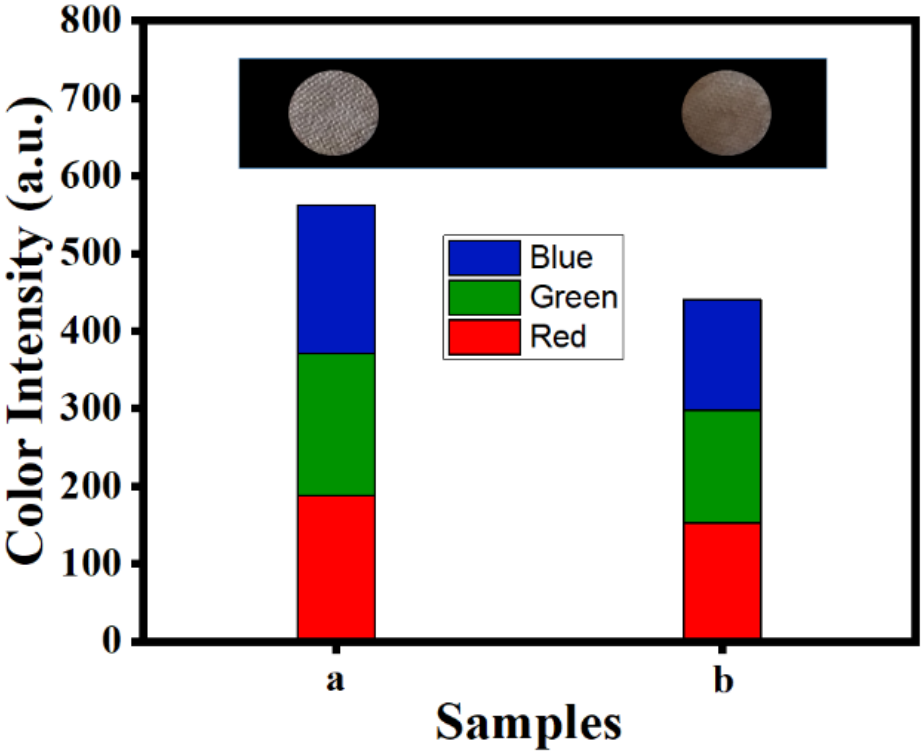

Figure 4.12: Evaluation of Red, Green, and Blue color properties of Ag NPs gel-coated fabric (a) in the absence and (b) in the presence of H_2S (aq.)

4.4 3D Printing and Characteristics of 3D-PMT

After testing the colorimetric response of the prepared inks, a fish-shaped sensor comprising three parts (head, body, and tail) was modeled using Autodesk software (Tinkercad). Before using the actual inks, the extrusion of previously prepared gel (5% (w/v)) through nozzles of different sizes was tested. It was found that the 0.41 mm nozzle at a flow speed of 1.5 mm/s was suitable for printing. The head, body, and tail were printed on a fabric substrate using Ag NPs gel, RA-MOF gel, and Cur-MOF gel, respectively.

To test the colorimetric response of 3D-PMTs, a simulated food package environment was created in six boxes by adding buffer solutions (3 mL) of different pH (3.0–11.0) and H_2S (aq.) of varying volumes (0.6–1.0 mL) in each box. Interestingly, the 3D-PMTs showed excellent colorimetric response in the simulated food package environment, even without direct contact with the solutions in the boxes, indicating their multi-responsive capabilities of detecting alkaline pH shift and H_2S gas. The color of the tail (Cur-MOF) appeared yellowish at pH 3.0–7.5, shifted to orange in extreme alkaline conditions at pH 10.0–11.0. Whereas the body part (RA-MOF) of the 3D-PMTs appeared pale pink at pH 3.0–7.5, it shifted to green in extreme alkaline conditions at pH 10.0–11.0. The head (Ag NPs) responded to varying volumes of H_2S (aq.) by distinct color transitions.

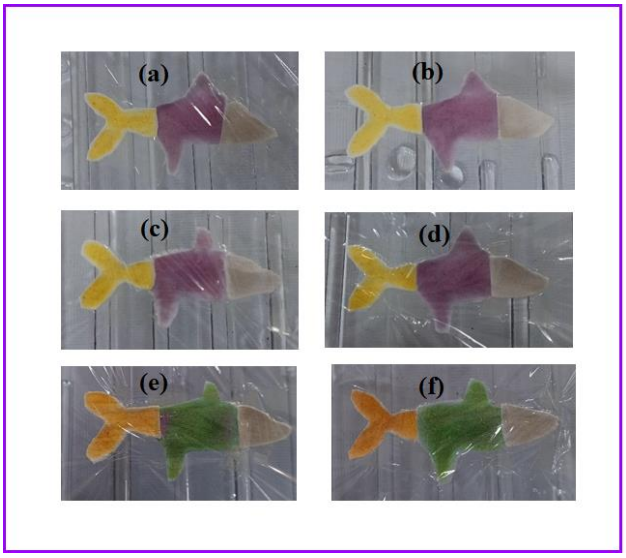

Tag no.	pH	H_2S (mL)
a	3.0	0.7
b	4.5	0.9
c	7.0	1.0
d	7.5	0.8
e	10.0	0.7
f	11.0	0.5

Figure 4.13: Colorimetric response of 3D-PMTs in a sealed environment containing buffers of different pH and H_2S (aq.) of varying volumes

Real-time colorimetric response and gas sensing capabilities of the 3D-PMT were examined under a simulated fish spoilage environment. The sensitivity was calculated using equation (1) after every 4-minute interval. The vapors of ammonia and hydrogen sulfide entered the porous substrate (fabric) and interacted with the dyes (RA and Cur) incorporated into the MOF along with Ag NPs. All the parts (head, body, and tail) of the 3D-PMT changed their color within 4 min due to their interactions with vapors as follows: tail (Cur-MOF), from yellowish to orange; body (RA-MOF), from pale pink to greenish; head (Ag NPs), from light brown to yellowish. Among all the parts (head, body, tail) of 3D-PMT, the RA-MOF displayed the maximum percentage sensitivity (S_{max} %) of about 29.94% after 8 min, while Ag NPs had the least S_{max} % value (9.90%) after 20 min.

After successfully testing the colorimetric response and reactivity of 3D-PMTs, the stability of the 3D-PMTs was tested to be used for a prolonged period of time. The color difference of the 3D-PMTs was calculated using equation (2). Interestingly, the colorimetric response was nearly similar each week, indicating the 3D-PMTs are highly stable and sensitive even for a longer period of time. All these characteristics demonstrate that these 3D-PMTs have the potential to be used for fish freshness monitoring.

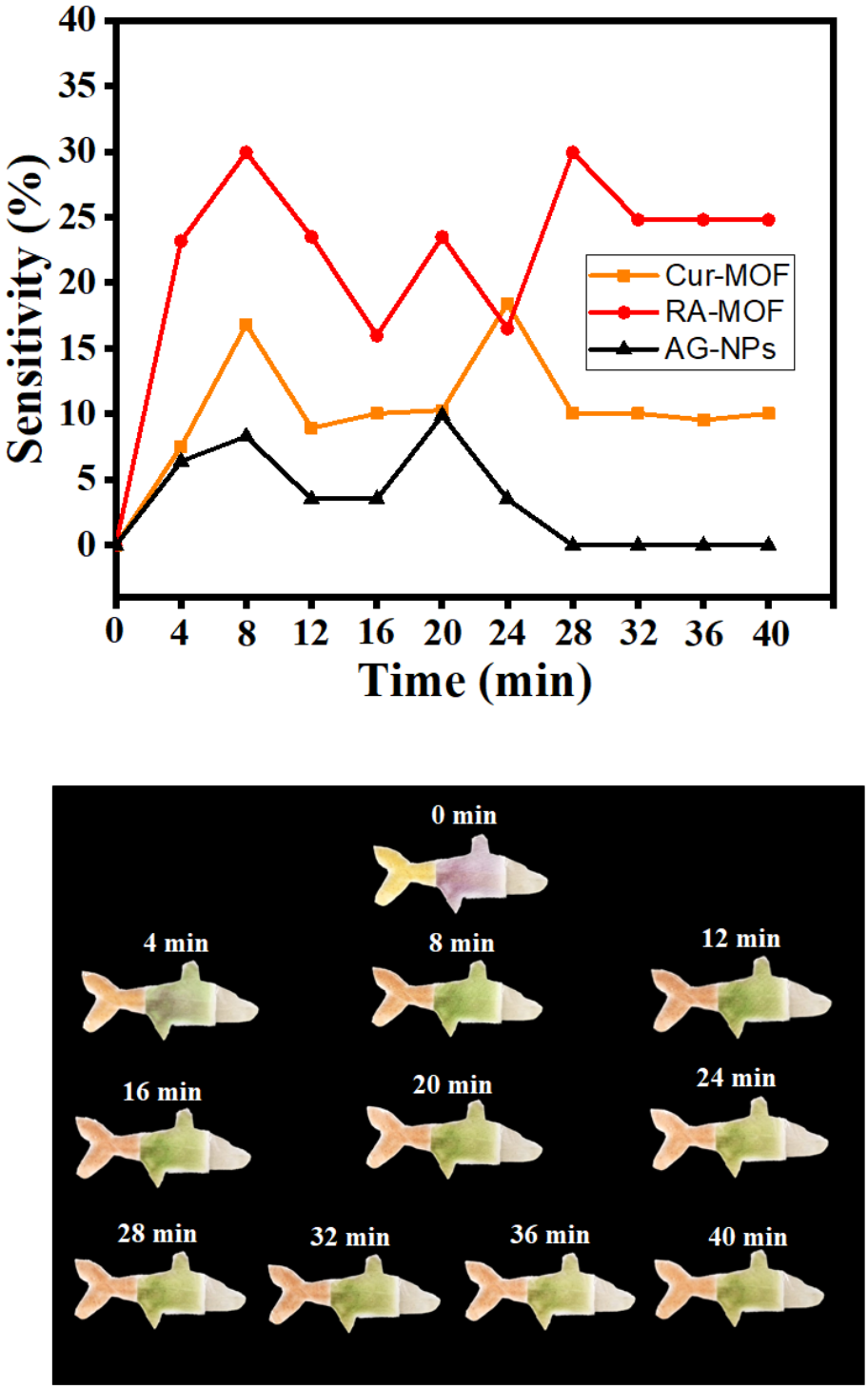

Figure 4.14: Sensitivity (%) and actual color changes of 3D-PMT when exposed to NH_4OH and H_2S in a sealed environment

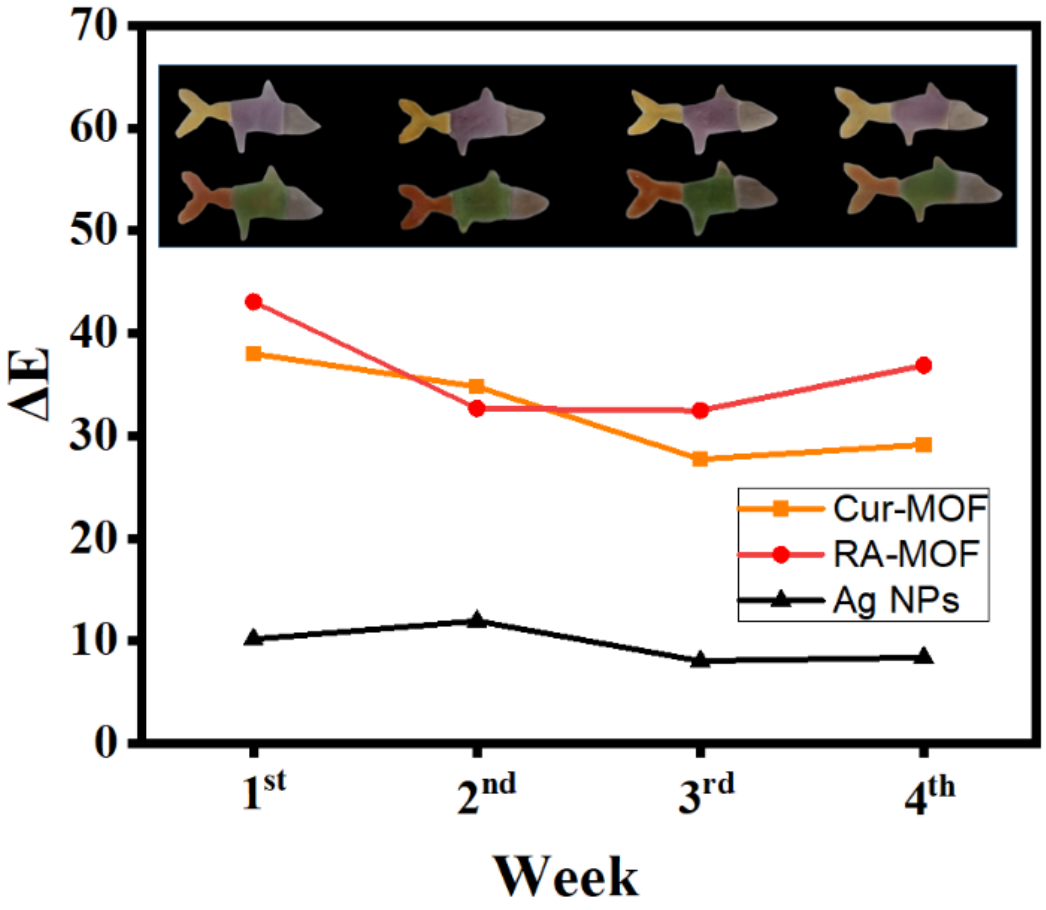

Figure 4.15: Storage Stability of 3D-PMTs over a period of four weeks

4.5 Application of 3D-PMT for Fish Freshness Monitoring

We tested our 3D-PMTs with fish samples at three different temperatures (30°C, 16°C, and -4°C) as shown in figure below. The 3D-PMTs were affixed to the inner side of the cling films and exposed to TVB-N in the headspace of the boxes. Interestingly, the 3D-PMTs responded by changing their colors at all the storage temperatures corresponding to the increase in concentration of TVB-N and hydrogen sulfide. Among all the parts of the 3D-PMT, the body (RA-MOF) has shown significant changes in color at all the storage temperatures. The room temperature (30°) results are as follows: It appeared pale pink at 0 h, indicating the fish is fresh; green at 24 h, suggesting the fish is deteriorating, and greenish yellow at >48 h, indicating the fish is highly spoiled. The body (RA-MOF) changed its color from pale pink to violet on the fourth day of storage at 16°C, indicating the initial spoilage stage. While the fish became inedible on the eighth day of storage, indicated by the greenish color of the body (RA-MOF). Interestingly, the shelf life of the fish increased during storage due to slow microbial growth at -4°C, indicated by the gradual color shifts of 3D-PMTs. The fish was consumable till the sixth week, as the body (RA-MOF) appeared pale pink. It started to deteriorate during the seventh week, indicated by the color transition of the 3D-PMT.

It is to be noted that the tail and head parts of the 3D-PMTs also responded to the shifts in the package environment. The head changed its color from brown to yellowish, indicating the release of hydrogen sulfide. The tail changed its color from yellowish to orange, indicating alkaline conditions in the package. All these results suggest that the 3D-PMT has great potential to predict the shelf life of the fish during all storage temperatures.

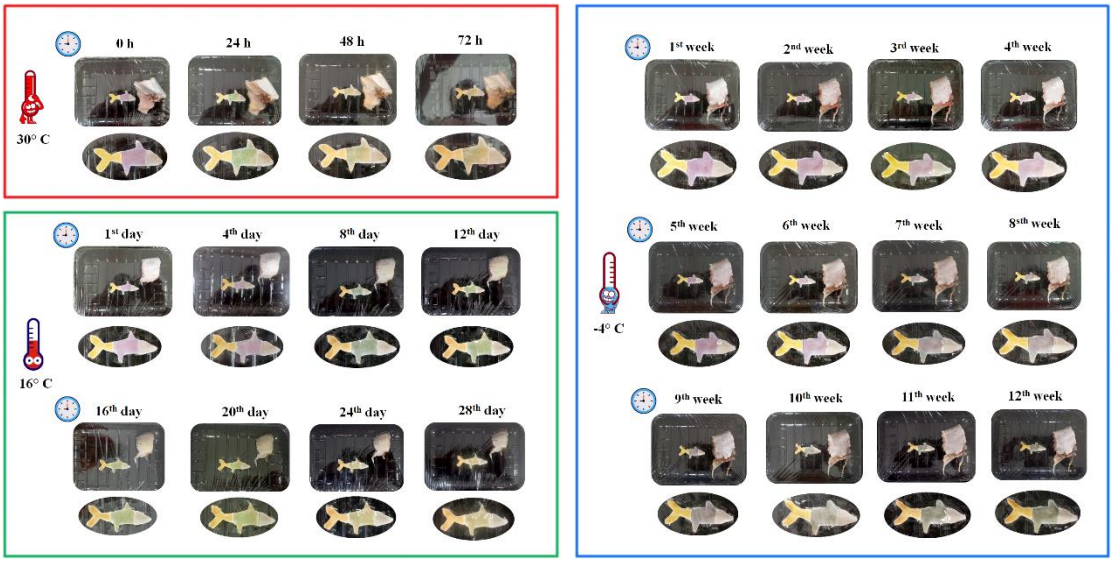

Figure 4.16: Real-time fish freshness monitoring at 30°C, 16°C, and -4°C

Chapter 5

Conclusion

In summary, we developed a multiplex tag on a fabric substrate via 3D printing technology to monitor the real-time freshness of packaged fish. The printable inks were prepared by mixing the RA-MOF (pH indicator), Cur-MOF (pH indicator), and Ag NPs (H_2S indicator) with cross-linked SA gel. The colorimetric properties of the materials were not affected by mixing with the SA gel and were visible to the naked eye. The 3D-PMTs displayed excellent sensitivity towards ammonia and hydrogen sulfide, and were stable even for a long storage period.

Moreover, we tested our 3D-PMTs with real fish samples at different storage temperatures. The shelf life of the fish was increased at -4°C, indicated by gradual color shifts of the 3D-PMT. Among all the parts of the 3D-PMT, the body part (RA-MOF) exhibited a broader range of color transitions at all the tested storage temperatures. These findings indicate that 3D printed gels have great potential in sensing applications at a broader range of temperatures and for a prolonged period of time.

References

1. Song, D., et al., 3D-printed flexible sensors for food monitoring. Chemical Engineering Journal, 2023. **474**: p. 146011.
2. Li, J., et al., 3D printing of hydrogels: Rational design strategies and emerging biomedical applications. Materials Science and Engineering: R: Reports, 2020. **140**: p. 100543.
3. Attaran, M., The rise of 3-D printing: The advantages of additive manufacturing over traditional manufacturing. Business horizons, 2017. **60**(5): p. 677-688.
4. Praveena, B., et al., A comprehensive review of emerging additive manufacturing (3D printing technology): Methods, materials, applications, challenges, trends and future potential. Materials Today: Proceedings, 2022. **52**: p. 1309-1313.
5. Xu, Y., et al., The boom in 3D-printed sensor technology. Sensors, 2017. **17**(5): p. 1166.
6. Karakurt, I. and L. Lin, 3D printing technologies: techniques, materials, and post-processing. Current Opinion in Chemical Engineering, 2020. **28**: p. 134-143.
7. Zhou, H.-C., J.R. Long, and O.M. Yaghi, Introduction to metal–organic frameworks. 2012, ACS Publications. p. 673-674.
8. Kuppler, R.J., et al., Potential applications of metal-organic frameworks. Coordination Chemistry Reviews, 2009. **253**(23-24): p. 3042-3066.
9. Kumar, P., A. Deep, and K.-H. Kim, Metal organic frameworks for sensing applications. TrAC Trends in Analytical Chemistry, 2015. **73**: p. 39-53.
10. Shao, G., et al., Tunable arrangement of hydrogel and cyclodextrin-based metal organic frameworks suitable for drug encapsulation and release. Carbohydrate Polymers, 2022. **278**: p. 118915.
11. Zhao, R.-n., et al., Cyclodextrin-based metal-organic framework materials: Classifications, synthesis strategies and applications in variegated delivery systems. Carbohydrate Polymers, 2023. **319**: p. 121198.
12. Ensafi, A.A., An introduction to sensors and biosensors, in Electrochemical biosensors. 2019, Elsevier. p. 1-10.
13. Javaid, M., et al., Sensors for daily life: A review. Sensors International, 2021. **2**: p. 100121.

14. Burger, J. and M. Gochfeld, Perceptions of the risks and benefits of fish consumption: Individual choices to reduce risk and increase health benefits. Environmental research, 2009. **109**(3): p. 343-349.
15. Ghaly, A.E., et al., Fish spoilage mechanisms and preservation techniques. American journal of applied sciences, 2010. **7**(7): p. 859.
16. Hassoun, A., et al., Fluorescence spectroscopy as a rapid and non-destructive method for monitoring quality and authenticity of fish and meat products: Impact of different preservation conditions. Lwt, 2019. **103**: p. 279-292.
17. Gram, L. and P. Dalgaard, Fish spoilage bacteria–problems and solutions. Current opinion in biotechnology, 2002. **13**(3): p. 262-266.
18. Peivasteh-Roudsari, L., et al., Occurrence of histamine in canned fish samples (Tuna, Sardine, Kilka, and Mackerel) from markets in Tehran. Journal of food protection, 2020. **83**(1): p. 136-141.
19. Liu, X., et al., An on-package colorimetric sensing label based on a sol-gel matrix for fish freshness monitoring. Food chemistry, 2020. **307**: p. 125580.
20. Zhai, X., et al., Novel colorimetric films based on starch/polyvinyl alcohol incorporated with roselle anthocyanins for fish freshness monitoring. Food Hydrocolloids, 2017. **69**: p. 308-317.
21. Cheng, J.-H., et al., Non-destructive and rapid determination of TVB-N content for freshness evaluation of grass carp (Ctenopharyngodon idella) by hyperspectral imaging. Innovative Food Science & Emerging Technologies, 2014. **21**: p. 179-187.
22. Taheri-Garavand, A., et al., Real-time nondestructive monitoring of Common Carp Fish freshness using robust vision-based intelligent modeling approaches. Computers and Electronics in Agriculture, 2019. **159**: p. 16-27.
23. Tang, T., et al., 3D printed curcumin-based composite film for monitoring fish freshness. Food Packaging and Shelf Life, 2024. **43**: p. 101289.
24. Huang, Y., et al., Preparation of 3D-Printed Intelligent Label Loading with Natural Pigment Nanoparticles and Its Freshness Monitoring Application. ACS Applied Bio Materials, 2025. **8**(8): p. 7504-7512.
25. Ghosh, S., et al., Natural colorants from plant pigments and their encapsulation: An emerging window for the food industry. Lwt, 2022. **153**: p. 112527.

26. Mohseni-Shahri, F.S., et al., ZnGlu MOF-enhanced anthocyanin-gelatin films: A novel approach for monitoring chicken meat freshness through experimental and molecular dynamics insights. Food chemistry, 2025. **475**: p. 143380.
27. Pang, H., et al., Active cellulose acetate/purple sweet potato anthocyanins@ cyclodextrin metal-organic framework/eugenol colorimetric film for pork preservation. International Journal of Biological Macromolecules, 2024. **263**: p. 130523.
28. Chen, H.-z., et al., Novel pH-sensitive films containing curcumin and anthocyanins to monitor fish freshness. Food Hydrocolloids, 2020. **100**: p. 105438.
29. Oidtmann, J., et al., Preparation and comparative release characteristics of three anthocyanin encapsulation systems. Journal of agricultural and food chemistry, 2012. **60**(3): p. 844-851.
30. Fang, J.-L., et al., Preparation and evaluation of an encapsulated anthocyanin complex for enhancing the stability of anthocyanin. Lwt, 2020. **117**: p. 108543.
31. Popoola, O., et al., Smart and sustainable 3D-printed nanocellulose-based sensors for food freshness monitoring. ACS Applied Materials & Interfaces, 2024. **16**(44): p. 60920-60932.
32. Tang, T., et al., Real-time freshness monitoring of fruits and vegetables integrating 3D-printed alginate-based colorimetric sensors with deep convolutional neural networks. Chemical Engineering Journal, 2025: p. 166387.
33. Chen, Y., et al., Extrusion-based 3D printing of pickering high internal phase emulsions stabilized by flaxseed protein-sodium alginate complexes for encapsulating curcumin. Colloids and Surfaces A: Physicochemical and Engineering Aspects, 2023. **673**: p. 131863.
34. Bao, Y., et al., A starch-based 3D printed intelligent colorimetric film co-loaded natural pigments for visualizing food freshness: Effect of nozzle size on gel structure formation. Food Hydrocolloids, 2024. **155**: p. 110218.
35. Hu, Y. and X. Maimaitiyiming, Gelatin/sodium alginate-based strongly adhesive, environmentally resistant, highly stable hydrogel for 3D printing to prepare multifunctional sensors and flexible supercapacitors. International Journal of Biological Macromolecules, 2024. **278**: p. 134712.

36. Tang, Q., et al., Novel ammonia-responsive carboxymethyl cellulose/Co-MOF multifunctional films for real-time visual monitoring of seafood freshness. International Journal of Biological Macromolecules, 2023. **230**: p. 123129.
37. Xu, R., et al., High-performance carboxymethyl starch/PVA based intelligent packaging films engineered with Cu-Trp nanocrystal as functional compatibilizer. Food Chemistry, 2024. **454**: p. 139696.
38. Zhang, K., et al., Aerogel colorimetric label sensors based on carboxymethyl cellulose/sodium alginate with black goji anthocyanin for monitoring fish freshness. International Journal of Biological Macromolecules, 2024. **265**: p. 130466.
39. Fang, H., et al., Multifunctional metal-organic framework-enhanced sodium alginate-based intelligent indicator: Mechanism and application for freshness monitoring. International Journal of Biological Macromolecules, 2024. **276**: p. 133914.
40. Tavakoli, S., et al., Novel intelligent films containing anthocyanin and phycocyanin for nondestructively tracing fish spoilage. Food Chemistry, 2023. **402**: p. 134203.
41. Awan, M., et al., A sandwich electrochemical immunosensor based on antibody functionalized-silver nanoparticles (Ab-Ag NPs) for the detection of dengue biomarker protein NS1. Journal of Molecular Liquids, 2020. **317**: p. 114014.
42. Hajra, S., et al., A green metal–organic framework-cyclodextrin mof: a novel multifunctional material based triboelectric nanogenerator for highly efficient mechanical energy harvesting. Advanced Functional Materials, 2021. **31**(28): p. 2101829.
43. Kang, S., et al., Colorimetric film based on polyvinyl alcohol/okra mucilage polysaccharide incorporated with rose anthocyanins for shrimp freshness monitoring. Carbohydrate Polymers, 2020. **229**: p. 115402.
44. Zhang, Y., et al., Citric acid modified β-cyclodextrin for the synthesis of water-stable and recoverable CD-MOF with enhanced adsorption sites: efficient removal of Congo red and copper ions from wastewater. Journal of Environmental Chemical Engineering, 2023. **11**(6): p. 111413.
45. Aldawsari, M.F. and M.K. Anwer, Synthesis of acalabrutinib loaded β-cyclodextrin-based metal–organic frameworks as a potential material for breast cancer therapy. Results in Chemistry, 2025: p. 102512.

46. Shahzaib, A., et al., Ultrarapid and highly efficient reduction of nitroaromatic compounds using cyclodextrin MOF. Catalysis Communications, 2023. **174**: p. 106569.
47. Jiang, L., et al., Encapsulation of catechin into nano-cyclodextrin-metal-organic frameworks: Preparation, characterization, and evaluation of storage stability and bioavailability. Food Chemistry, 2022. **394**: p. 133553.
48. Ferreira, M.E., et al., Mode-Selective Raman Imaging of Metal–Organic Frameworks Reveals Surface Heterogeneities of Single HKUST-1 Crystals. ACS omega, 2025. **10**(30): p. 33393.
49. Li, W., et al., Spectroscopic and theoretical study on inclusion complexation of beta-cyclodextrin with permethrin. Journal of Molecular Structure, 2010. **981**(1-3): p. 194-203.
50. Krishnaswamy, K., V. Orsat, and K. Thangavel, Synthesis and characterization of nano-encapsulated catechin by molecular inclusion with beta-cyclodextrin. Journal of Food Engineering, 2012. **111**(2): p. 255-264.
51. Ramzan, M., et al., Synthesis and analytical characterization of Ca-BTC metal organic framework. Heliyon, 2023. **9**(11).
52. Zaffino, C., B. Russo, and S. Bruni, Surface-enhanced Raman scattering (SERS) study of anthocyanidins. Spectrochimica Acta Part A: Molecular and Biomolecular Spectroscopy, 2015. **149**: p. 41-47.
53. Peng, Q., et al., Rapid determination of turmeric roots quality based on the Raman spectrum of curcumin. Food analytical methods, 2015. **8**(1): p. 103-108.
54. del Castillo, M.L.R., et al., Stabilization of curcumin against photodegradation by encapsulation in gamma-cyclodextrin: A study based on chromatographic and spectroscopic (Raman and UV–visible) data. Vibrational Spectroscopy, 2015. **81**: p. 106-111.
55. Bhattacharjee, T., et al., Synthesis and characterization of exfoliated beta-cyclodextrin functionalized graphene oxide for adsorptive removal of atenolol. Materials Chemistry and Physics, 2022. **288**: p. 126413.
56. Al-Harbi, S.A. and Y.Q. Almulaiky, Cu-trimesic acid-based metal organic frameworks for improved ß-galactosidase immobilization: enhanced stability, reusability and lactose hydrolysis. Journal of Molecular Liquids, 2023. **392**: p. 123456.

57. Moussa, Z., et al., Encapsulation of curcumin in cyclodextrin-metal organic frameworks: Dissociation of loaded CD-MOFs enhances stability of curcumin. Food chemistry, 2016. **212**: p. 485-494.
58. Luo, X. and L.-T. Lim, Curcumin-loaded electrospun nonwoven as a colorimetric indicator for volatile amines. Lwt, 2020. **128**: p. 109493.
59. Xiaowei, H., et al., Fabrication and characterization of colorimetric indicator for Salmon freshness monitoring using agar/polyvinyl alcohol gel and anthocyanin from different plant sources. International Journal of Biological Macromolecules, 2023. **239**: p. 124198.
60. Wu, Y., Y. Gao, and C. Li, Preparation and characterization of smart indicator films based on gellan gum/modified black rice anthocyanin/curcumin for improving the stability of natural anthocyanins. International Journal of Biological Macromolecules, 2023. **253**: p. 127436.
61. Liu, J., et al., Films based on κ-carrageenan incorporated with curcumin for freshness monitoring. Food Hydrocolloids, 2018. **83**: p. 134-142.
62. Chen, R., H.R. Morris, and P.M. Whitmore, Fast detection of hydrogen sulfide gas in the ppmv range with silver nanoparticle films at ambient conditions. Sensors and Actuators B: Chemical, 2013. **186**: p. 431-438.